Contents lists available at ScienceDirect

Heliyon

Research article

Simulation of carbon dioxide mineralization and its effect on fault leakage rates in the South Georgia rift basin, southeastern U.S.

Adil Alshammari [a,*], Venkat Lakshmi [b], Duke Brantley [a], Camelia C. Knapp [c], James H. Knapp [c]

[a] School of the Earth, Ocean, and Environment, University of South Carolina, United States
[b] Department of Engineering Systems and Environment, University of Virginia, United States
[c] School of Geology, Noble Research Center, Oklahoma State University, United States

ABSTRACT

Over the past few decades, measured levels of atmospheric carbon dioxide have substantially increased. One of the ways to limit the adverse impacts of increased carbon dioxide concentrations is to capture and store it inside Earth's subsurface, a process known as CO_2 sequestration. The success of this method is critically dependent on the ability to confine injected CO_2 for up to thousands of years. Establishing effective maintenance of sealing systems of reservoirs is of importance to prevent CO_2 leakage. In addition, understanding the nature and rate of potential CO_2 leakage related to this injection process is essential to evaluating seal effectiveness and ultimately mitigating global warming.

In this study, we evaluated the impact of common chemical reactions between CO_2 and subsurface materials in situ as well as the relationship between CO_2 plume distribution and the CO_2 leakage within the seal zone that cause mineralization. Using subsurface seismic data and well log information, a three-dimensional model consisting of a reservoir and seal zones was created and evaluated for the South Georgia Rift (SGR) basin in the southeastern U.S. The Computer Modeling Group (CMG, 2017), was used to model the effect of CO_2 mineralization on the optimal values of fault permeability permeabilitydue to fluid substitution between the formation water and CO_2. The model simulated the chemical reactions between carbon dioxide and mafic minerals to produce stable minerals of carbonate rock that form in the fault. Preliminary results show that CO_2 migration can be controlled effectively for fault permeability values between 0.1-1 mD. Within this range, mineralization effectively reduced CO_2 leakage within the seal zone.

1. Introduction

Carbon dioxide emissions from the outpourings of the industrial revolution have polluted the Earth's atmosphere and threatened our ecosystem. The anthropogenic creation of these greenhouse gases is a prominent contributor to global warming which causes sea level rise and worsen many types of natural disasters (Bachu and Adams, 2003) (Melillo, 2014) (Stocker, 2014). Environmental scientists have suggested that carbon dioxide could be reduced by storing it in Earth's subsurface. According to the Department of Energy (DOE), saline formations, oil and gas reservoirs, coal seam, igneous rocks, and organic-rich shales could all be used for geological CO_2 storage. Each of these formations has unique features that allow for the storage of carbon dioxide (Holloway, 2007) (Khatiwada et al., 2012).

The South Georgia Rift (SGR) Basin contains igneous rocks that are ideal for storing carbon dioxide as they react with CO_2 to produce geochemically stable carbonate rock (Seifritz, 1990) (McGrail et al., 2006) (Alfredsson et al., 2008) (Oelkers et al., 2008) (Goldberg and Slagle, 2009) (Gislason, 2010). Igneous rocks with various geological structures and stratigraphy can serve as an ideal trap for carbon dioxide sequestration if there is a top and bottom seal, the rocks have an adequate porosity and permeability, and there is sufficient storage capacity (Khatiwada et al., 2012) (Goldberg et al., 2008) (Brantley et al., 2015). Unfortunately, as it is in the case of the South Georgia Rift Basin, it is hard to find a reservoir comprised of igneous rocks that has both sufficient capacity for carbon dioxide storage and is not impacted by tectonic activity such as folding/fracturing. Faults and fractures created by tectonic activity are considered a significant threat which undermine long term CO_2 storage. This is because they create weak areas in the caprock which allows CO_2 to escape from the igneous rock reservoir and into the atmosphere. However, utilizing mineralization in the weak areas mitigates CO_2 leakage in the SGR basin and allows for secure CO_2 storage Dabirian

---

* Corresponding author.
E-mail address: aalshammari@geol.sc.edu (A. Alshammari).

et al. (2012). Conducting risk assessments and monitoring CO_2 leakage is crucial to ensure that systems which employ mineralization are working effectively. Further, predicting CO_2 migration through structurally complex geology is an important research question that is essential to optimize global warming mitigation.

2. Geological background

Approximately 200M years ago, the breakup of Pangea throughout the Mesozoic era formed the North American continent. During the Triassic and Jurassic eras, the eastern portion of North American passive margin was formed (Marzoli et al., 1999) (Gutié rrez-Alonso et al., 2008). The SGR basin, located in the southeastern part of the North American margin (longitude 78°-87°W; latitude 30°–34° N), covers parts of Alabama, Georgia, Florida, and South Carolina, and extends to the offshore area of South Carolina (Figure 1). The maximum depth of the SGR basin is 5–6 km (Heffner, 2013), and it is filled primarily with continental sedimentary deposits as well as volcanic and igneous rock (McBride and Moslow, 1991). Sedimentary rocks in this area are in thick layers comprised of sandstone, siltstone, and clay and are separated by thin

layers of igneous rocks that consist of basalt and diabase. According to (King, 1971), the magmatic features vary between basalt flow, diabase dike, and sills, and cover a large area of the Central Atlantic magmatic province.

A series of NE-SW-oriented asymmetric half -grabens dominate the structure of the SGR basin and are separated by poorly defined NW-SE trending transfer zones (Klitgord et al., 1988) (Heffner, 2013). Major, basin-bounding growth faults place rift basin stratigraphy against pre-Mesozoic rocks and form lateral boundaries for the rift sedimentary rocks could invested in the environmental treatment efforts (Cumbest, 1998). Within the SGR basin, Weatherford Laboratories in Houston, Texas, have analyzed core samples from the Rizer #1 borehole which penetrated 1889 m of sequences of compressed sandstone and diabase and showed acceptable values of porosity and permeability (10% and 200 mD, respectively) for CO_2 storage. The diabase unites already affected by highly fractured process due to tectonic activities during Mesozoic time and that supported the geophysical log values of porosity and permeability. In addition, water flowed in to borehole from the diabase unite during the drilling Rizer#1 borehole is confirmed the assumption of using diabase as reservoir (Brantley et al., 2015). The
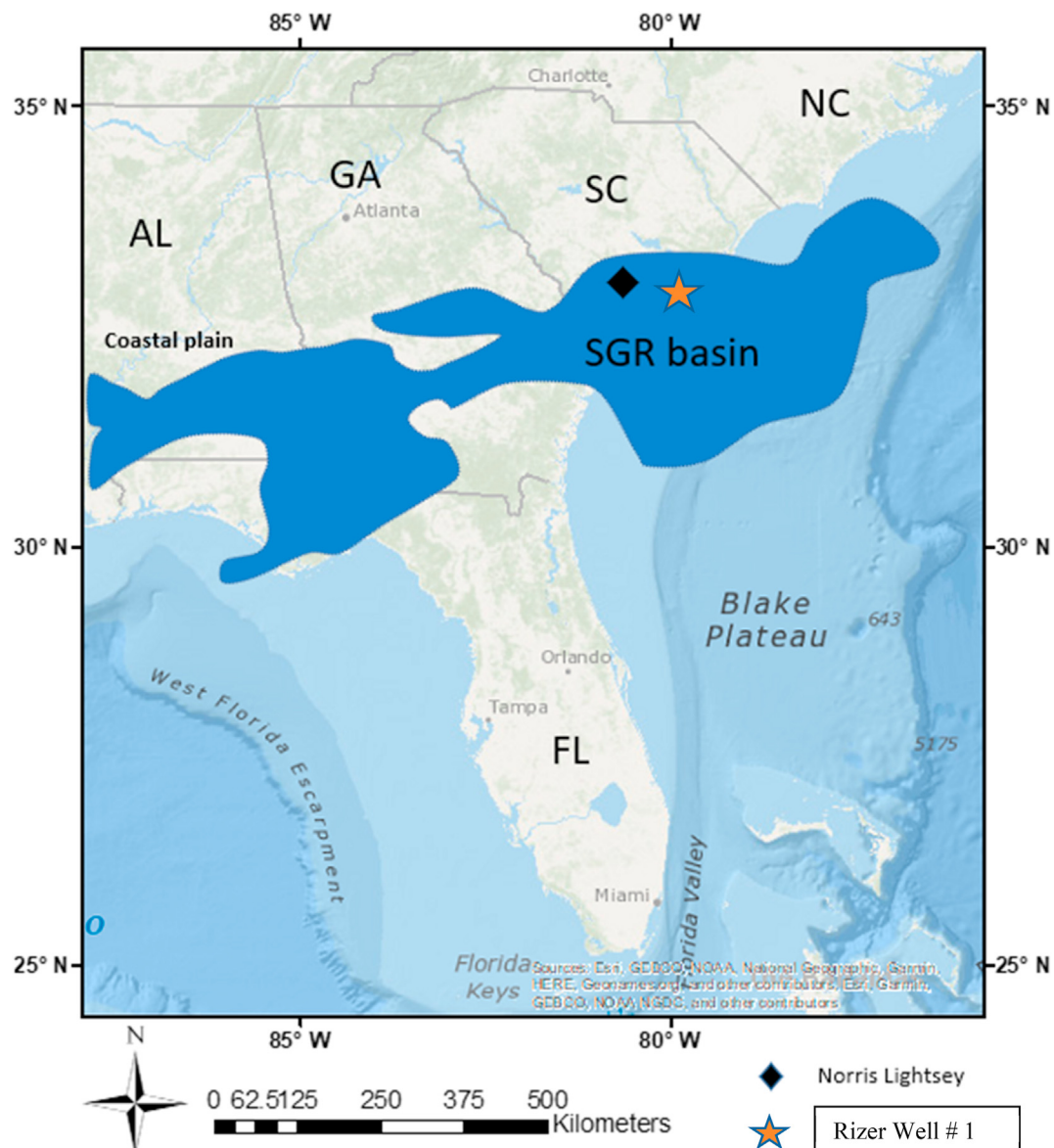
Figure 1. Location of the South Georgia Rift Basin (SGR). The area covered by the SGR is indicated by dark blue. The location of the Norris Lightsey #1 and Rizer Well #1 boreholes is marked by a diamond and a star, respectively. The map is modified from that previously included in Heffner (2013).

Norris Lightsey #1 well, drilled to a depth of 4,000 m, showed fluvial deposits and coastal plain sediments for the first 600-meters from the surface. Below this, there is frequently a sequence between the sedimentary and the igneous rocks through the geological column that were formed during Triassic and Jurassic Period. This sequensecsv are affected by tectonic activities; faults and folds (Figure 2). The thick sedimentary rocks serve as a seal to while the thin layers of igneous rock that act as a reservoir for CO₂ storage, qualifying the SGR basin efficient for CO₂ storage (Rine et al., 2014).

Based on the geological and petrophysical characteristics obtained from the borehole analyses, the sequence of Triassic red beds/Jurassic basalt and diabase in the SGR basin have the best potential as CO₂ injection zones (Heffner, 2013)and (Brantley et al., 2015). This is because there is a thick seal or caprock of sedimentary rocks graded in grain size from sandstone, siltstone, shale, and claystone serve as seal while a thin layer of igneous rock that serves as a CO₂ reservoir according to porosity and permeability values. . The sedimentary rocks that include layers of shale have a relatively low porosity and permeability of 0.34% and 0.00065 mD, respectively, on the other hand, the igneous rock already associated with breakup of Pangea in the early Mesozoic which volcanic and tectonic activity like faults support the rifting process and that could increase the fractured porosity in the SGR basin (Figure 3) (Marzoli et al., 1999)These values in igneous rocks are increased and can be up to 14% porosity and 200 mD permeability.

During the Triassic period, before sedimentary rock was deposited, faults resulting from tectonic activity that created the SGR basin enhanced the permeability of the igneous rock. This is evidenced by water that was observed as flowing from the diabase horizon and the fractures observed in the Rizer #1 borehole (Brantley et al., 2015). In addition, porosity and permeability tend to increase in areas that are affected by faults and weathering (Ziegler, 2012). Because of this, it is important to incorporate a range of fault permeabilities into the model that are compatible with the heterogeneity of igneous rock. Despite the SGR's large capacity for CO₂ storage and its onshore location, the risks of leakage from faults and fractures threaten the feasibility of CO₂ storage in the basin. CO₂ mineralization in these faults and fractures reduces that risk and provides an opportunity of CO₂ storage in a safe phase.

3. Considerations for effective mineralization

Predicting leakage areas, estimating the time at which leakage occurs, and fault hydraulic properties are not yet fully understood. Simulation modeling studies are required to support the importance of identifying key permeability values that allow for the seal to be effective in containing CO₂ in the reservoir (Akintunde et al., 2017).

There were two main scientific questions addressed in this study. The first question investigated the distribution of the CO₂ plume with respect to the variation of fault permeability as well as the critical values of permeability and their impact on the CO₂ plume migration. The heterogeneity of the petrophysical features such as porosity and permeability contributed to defining the relationship between the CO₂ and its contact with the formation water. Within portions of the resrvoir that are comprised of active porosity, if the plume migration was relatively small it was a result of a large volumetric displacement of formation water by CO₂. The opposite is true for a large plume migration and a small volumetric displacement (Frailey and Leetaru, 2009). At the same time, the vertical migration of the CO₂ plume was affected by the heterogeneity of the reservoir which was directly related to the reservoir's variation of porosity and permeability (Pan et al., 2009). Consequently, understanding the nature of the CO₂ plume distribution comes from understanding many interdependent parameters including porosity and permeability (Nicol et al., 2017). Applying a logarithmic scale approach for fault permeability resulted in important gaps of information regarding how the CO₂ plume migrated with respect to variations in permeability in smaller increments (Brantley et al., 2015). This led to a more careful investigation that paid attention to the effects of smaller

increments of fault permeability on CO₂ plume migration. Without first determining the critical values of fault permeability in which mineralization is successful, applying the mineralization concept in a model would not be effective. This is because some values of permeability are not appropriate for CO₂ sequestration as applying mineralization in those scenarios does not reduce CO₂ leakage into the atmosphere.

The second question investigated in this study examined applying mineralization to a model and using interpolation to determine specific values of fault permeability that would provide reactions between CO₂ and igneous minerals. Formed in the Mesozoic era, the Central Atlantic Magmatic Province is comprised of basaltic rock that extends along the eastern seaboard of the United States. This formation is considered a good example of igneous rock that is distributed throughout several basins formed after rifting processes. Thick sedimentary deposits cover all igneous rock after rifting. These outputs provided a good example of a model study in SGR basin (Goldberg et al., 2010). Laboratory experiments performed on a core samples of basaltic rock and sandstone showed that under the pressure and temperature conditions 100 bar and 100 Co, respectively, carbonate minerals formed more quickly in the fracture network of the basaltic rock than the deep sandstone reservoir (Xiong et al., 2018). The injection of supercritical CO₂ into basaltic rock did not only reduce CO₂ emissions into the atmosphere but also served as a permanent way to store CO₂. In addition, CO₂ enhanced kinetic reactions to produce more stable carbonate minerals (Rosa and Rosa, 2012) (Khatiwada et al., 2012) (Snæbjörnsdóttir et al., 2014; Gislason et al., 2014). These reactions produced new carbonate rocks in fractured media within the fault zone. Exploring these questions allowed for the establishment of the critical values of fault permeability and an understanding of how these values impact the feasibility for mineralization and the reduction of fault leakage.

4. Methodology

Depending on conditions of the reservoir, CO₂ trapping can occur in supercritical, gas, liquid, and dissolution phases. Columbia river basalt group provide a data set for CO₂ mineralization. after CO₂ injection in basaltic and ultramafic rock, the dissolution of CO₂ by formation water rapidly, then cations extracted from the basalt and increased gradually before the mineralization occures (Gislason et al., 2014) (Schaef and McGrail, 2009). Through mineralization trapping, which is the goal of this study, CO₂ can exist in the solid phase when trapped in underground rock. A previous study of CO₂ sequestration in the SGR basin examined supercritical, gas, and liquid CO₂ phases of storage by applying logarithmic values of fault permeability in the range 0–1000 mD (Brantley et al., 2015). The study found that all values except zero within the range tested did not completely trap CO₂ in supercritical, liquid, and gas phases and allowed CO₂ to escape into the atmosphere. CO₂ sequestration is a viable solution for reducing global warming with respect to CO₂ emissions in the southeastern U.S. However, ensuring there is no leakage after CO₂ is sequestered is essential for successful storage. This study suggests that mineralization is a safe method for long-term storage of CO₂ that is able to reduce the CO₂ leakage through faults and consequently control the CO₂ plume migration.

A three-dimensional geological model of the SGR basin was built using Petrel software (Schlumberger, 2015) from seismic and borehole data (Rizer #1 and Norris-Lightsey #1) (Heffner, 2013) (Brantley et al., 2015). The geological model represents the SGR basin's complexity with respect to the overlap between the sedimentary and igneous strata and the tectonic forces that built a complicated fault system in the basin (Figure 3). To optimize the simulation time, a 3D simulation dynamic model was extracted from the geological model to demonstrate the CO₂ migration through permeable layers over time. There were many modifications to the model that included eliminating a wide distribution of similar faults, extracting the model grid to enhance simulation speed, and focusing on a single fault area. All these modification were made to accelerate the simulation speed especially when applying mineralization

Stratigraphic distribution of the Norris Lightsey #1 borehole
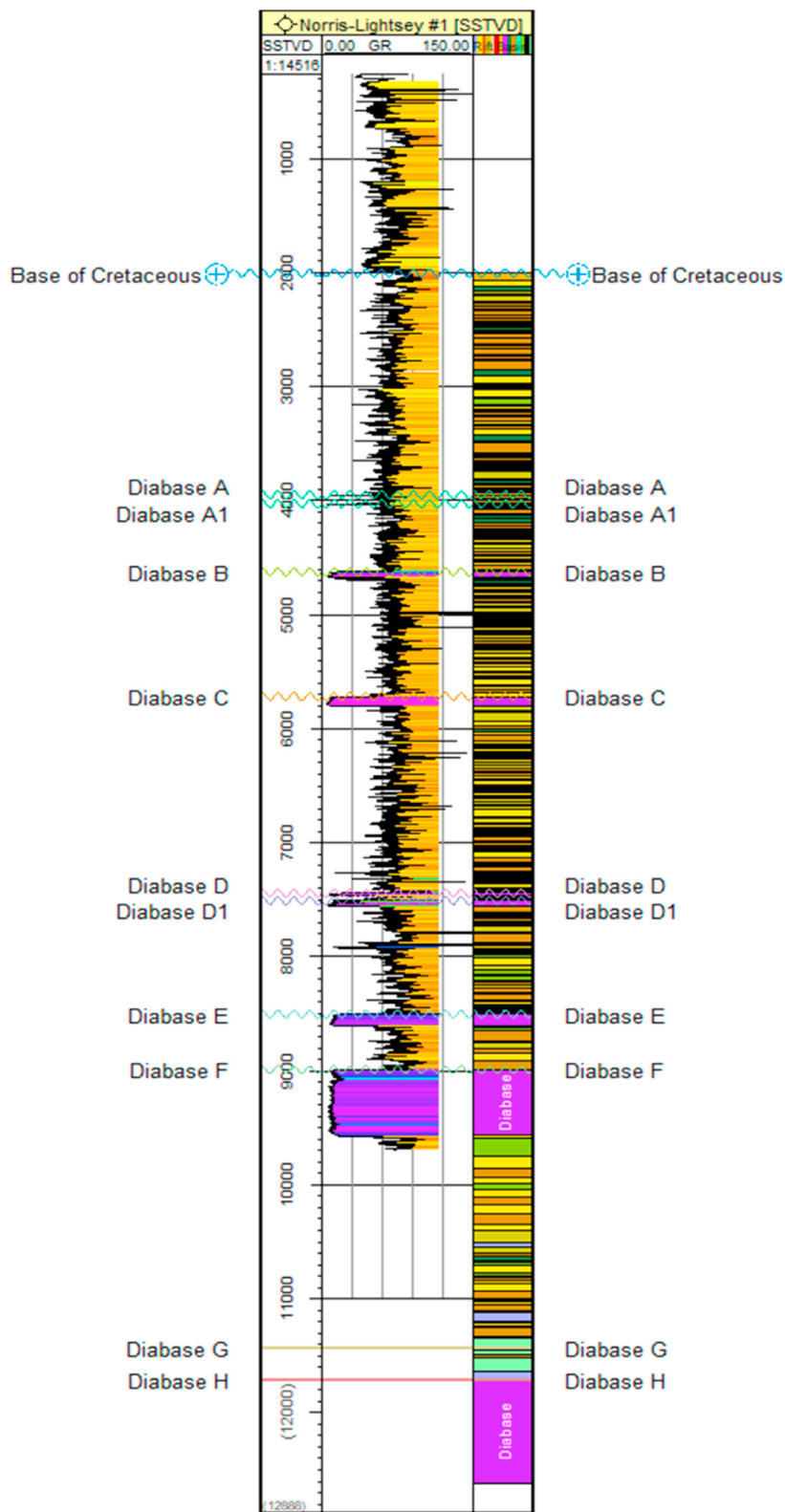
Figure 2. Stratigraphic distribution of the Norris Lightsey #1 borehole. The diabase rock is classified into several layers depending on the depth and thickness of seal. The target injection zone (Diabase E) is covered by a seal of sandstone, located at a depth of more than 800 m (a minimum depth for CO_2 storage), and extends widely within the study area. Thin diabase layers were eliminated for economic reasons. The thickest diabase layers (F,H) did not cover the entire study area and were not alone sufficient for carbon dioxide sequestration.
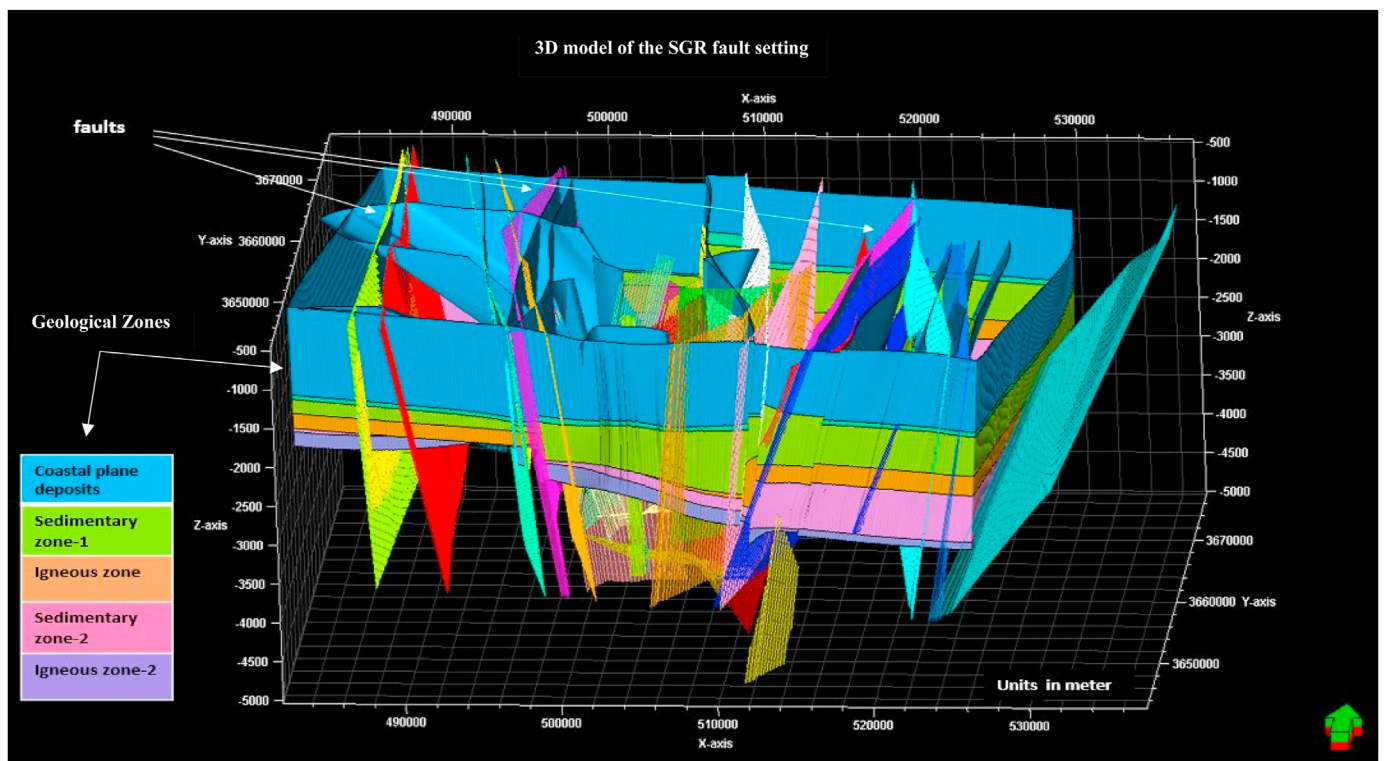
Figure 3. 3D model of the SGR displaying the orientation of faults, density, and the complexity of the geological settings due to tectonic activities. This figure was generated using Petrel 2014 software by analyzing the seismic and borehole data. The figure was modified from Brantley et al., (2015).

process in the second part of this research. Model simulation using the entire SGR basin area is time-consuming. Therefore, only the area that was covered by faults, which is a part of the entire SGR basin, was used in the simulation modeling for the SGR basin. sice the study focusing on the fault area only.

The 3-D simulation model used the CMG, 2017 software package was built using the following settings (Figure 4A and Table 1):

1. Five zones that started at a minimum depth of 1200m. Each zone included ten layers. The first (D-C), third (D-E), and fifth (D-F) zones had a wide range of igneous rock while the second (SSTN-1) and fourth (SSTN-2) zones were characterized by sedimentary rock. This classification was compatible with the sequences of sedimentary and igneous strata.
2. The sedimentary zones SSTN1 and SSTN2 were considered to be seal zones while the igneous zone D-E was considered to be an injection zone as it is surrounded vertically by two seals (Figure 4A and Figure 4B). All of these horizontal zones were intersected vertically with a range of permeability values for the fault zone.
3. The average porosity and permeability of sedimentary rocks that served as seals for the model were 0.34% and 0.00065 mD, respectively. For igneous rocks (the reservoir part of the model), porosity and permeability were designated to be 14% and 10 mD, respectively, as they have been affected by prior erosion and tectonic activities to a greater extent than the sedimentary rocks (Akintunde et al., 2013). The injection zone had a scaled permeability (from 0 to 200 mD) to reflect the heterogeneity of the petrophysical features and to match the lateral variability.
4. The fault permeability zone ranged from 0.1 mD (which provided the maximum resistance) to 1000 mD (which provided the minimum resistance) to cover the heterogeneity that exists in the basin.
5. CO_2 was injected in all layers of the third zone (D-E) where the zone intersected the fault.

6. The initial conditions at the top of the model were adjusted to 30 °C and 55 MPa or 8000 psi for temperature and pressure, respectively. This is will change during the injection period(Figure 5).
7. The simulation period started during the year of 2016 and extended to 2216. The volumetric injection rate of CO_2 was 10 M m³/year of supercritical CO_2 over 20 years. The well injection was then shut down, and the fate of the CO_2 was predicted though the simulation to 2216.
8. The resolution of the model was 172 by 148 grids for the 50 layers and covered the area around the fault.

5. Basic modeling of CO_2 plume migration

The purpose of studying the physical behavior of the CO_2 plume injected into a permeable fault is to recognize how leakage is influenced by both fault orientation and permeability. Understanding the CO_2 plume allows for the preparation of a model for mineralization processing. According to the Norris # 1 borehole stratigraphy, there was a small scale of depth distribution for the upper zone in the model between diabase layers C and E, which was accounted for in the model (Figure 2). The impact of temperature was not considered in the model because there is no information to support recent volcanic activity in the SGR basin (Figure 5). Consequently, leakage was considered to be a function of time if permeability was the only factor that allowed CO_2 to migrate to the top of the model through the seal. In Brantley's model, there was a wide range of logarithmic values used and it was concluded that all permeable faults have responded to CO_2 migration and caused leakage. This of course is because all fault permeability values except zero have caused leakage regardless of time or amount that leaked. Using a wide range of logarithmic values did not illustrate the potential for leakage from faults with a permeability ranging 0–1 mD, that consider a small values, to be sequestered using mineralization finally, which is the significance of this model.
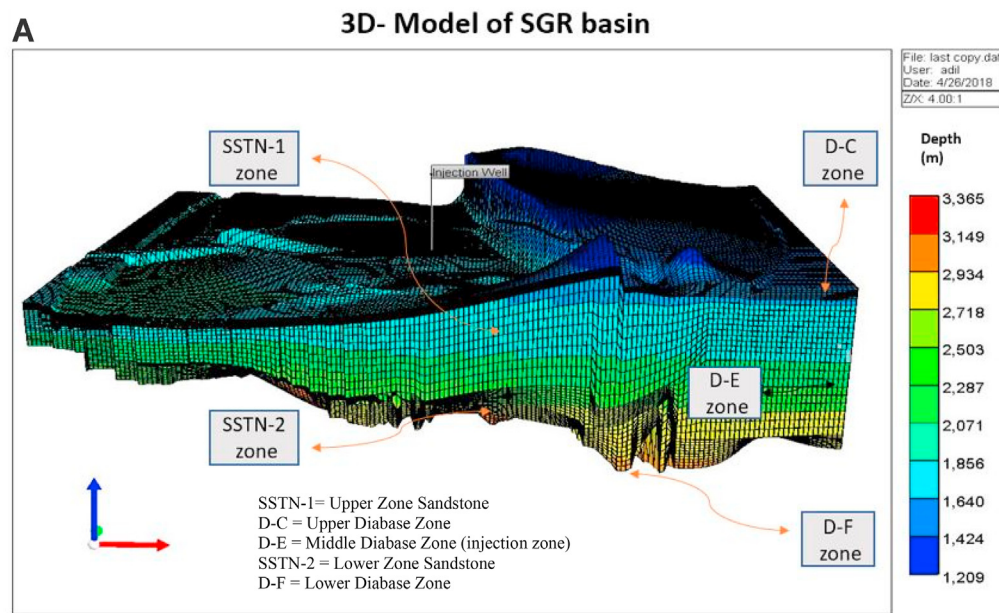
Figure 4. A. 3D CMG-model of the SGR basin. The SGR model was divided into five zones from top to bottom (D-C, SSTN-1, D-E, SSTN-2, D-F). The injection zone (D–E) was located in the middle of them model and surrounded vertically by two seal zones (SSTN-1 and SSTN-2). The model was comprised of a sequence of igneous and sedimentary rocks. B. 2D depiction of the location of embedded fault within the simulation model. The top view (X–Y) shows the fault indicated by red located between the top seal comprised of sandstone indicated by the blue area in the figure. The side view shows the red fault zone crossing the blue seal zones and green injection zone vertically. The area within the fault zone applied various permeability values during each simulation. The location of the injection well was placed close to the crest of anticline of the injection zone (D–E) to avoid the lateral migration of CO_2.
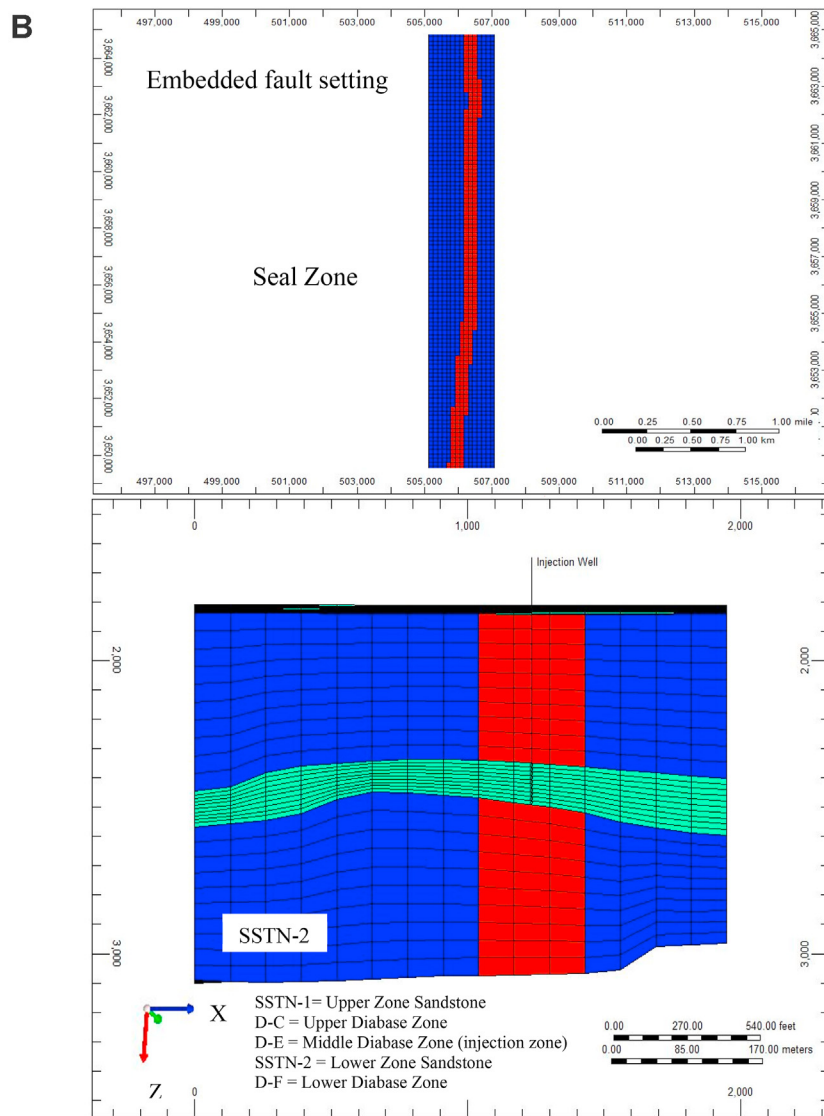
Table 1. Parameters for model simulation in SGR Basin. Each zone has ten layers and porosity and permeability values. The top of the model is Diabase –C while the bottom of the model is Diabase –F. The injection zone is Diabase -E, and the seal zones are sandstone one and two zones.

Injection simulation Model Set Up					
Material/Zone	50-layer total in the Model	Depth (m)Min/Max	Porosity (%)	Permeability (mD)	Notes
Diabase C	Layer 1-10	1283/1916	14	10	Top of model
Sandstone 1	Layer 11-20	1387/2848	3.4	0.00065	Seal
Diabase E	Layer 21-30	1710/2953	14	1-200 range	Injection Horizon
Sandstone 2	Layer 31-40	1710/3453	3.4	0.00065	Seal
Diabase F	Layer 41-50	1710/3517	14	10	Base of Model
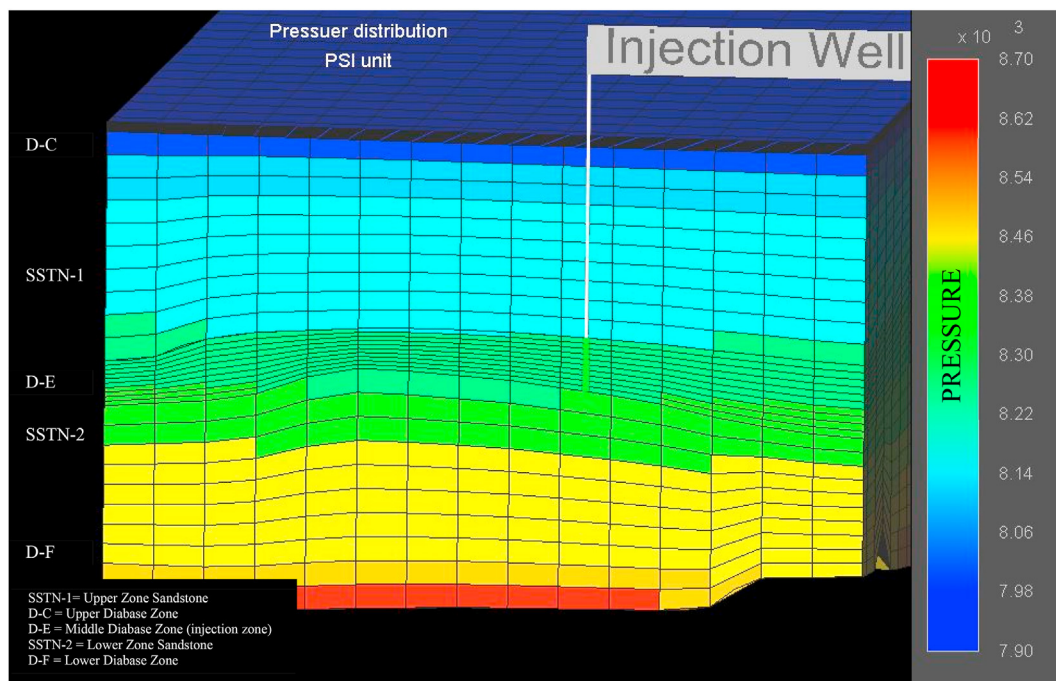
Figure 5. Pressure distribution of the model at initial conditions. The pressure at the bottom of the simulation model was 7.9×10^3 PSI which was equivalent to cumulative pressure in the beginning of simulation. The model was located at an approximate depth of 2000 m and the pressure at the injection zone was 8400 PSI.

Since mineralization trapping is slow and safe for long term storage, controlling CO_2 leakage time is vital to the success of mineralization storage. To ensure that there is sufficient time for mineralization, the CO_2 plume should be kept in the reservoir as long as possible. That could happen when small permeability values such as described critical values.

In the 3D model, a chemical reaction package Winprop 2017 was eliminated temporarily to determine critical values of fault permeability and the corresponding CO_2 migration response. After these values were determined, the package was then added to the model to assess mineralization conditions.

6. Chemical and mineral advanced modeling

Mineralization is an effective way to enhance the feasibility CO_2 sequestration. It helps fill fractured seals and reduces the permeability to minimize the risk of CO_2 leakage over time. The suggested models in the SGR basin designated in this study were assumed to be optimal for mineralization. It was assumed that the conditions allowed for mineralization to minimize leakage if it occurred in the fault zone and kept more of the CO_2 sequestrated in the mineral phase rather than the supercritical liquid and aqueous phases. In the models, a wide range of mineral components were used that included olivine, pyroxene, plagioclase, and orthoclase in diabase, basalt, and andesite igneous rocks. These minerals were affected differentially by weathering processes in the Jurassic era and then buried with thick layers of

sedimentary rocks such as sandstone, siltstone, and clay minerals. This was confirmed by flowing water observed in the basaltic layer during Rizer # 1 borehole drilling (Rine et al., 2014). A geochemical core sample was not available, so the result analysis of a sample taken from igneous rock deposits formed during the Jurassic era in a similar environment was used. Basalt rock core samples from the grand ronde formation were extracted at a 1022-meter depth and analyzed by the Northwest National Laboratory (Xiong et al., 2018). The core sample showed the percentage of primary minerals that comprised the sample (Table 2). Plagioclase comprised 58% of the sample. Consequently, anorthite, calcite, and kaolinite were considered to be the common carbonite mineral and clay mineral for the model. The plagioclase group was considered to be the source of calcium, magnesium, aluminum and other many cations that were needed in the model's mineralization reactions. Other minerals detected in the core sample that comprised a lower percentage were not considered for the model.

Table 2. Composition of geochemical minerals modified from (Xiong et al., 2018) Grand Ronde Basalt Sample Composition

Mineral	Composition (vol %)	Formula
plagioclase	58	Ca0.51 Na0.46 K0.03 Al1.47 Si2.49 O8
pyroxene	14	Mg0.72Fe0.59Ca0.60Si1.90Al0.12O6
ilmenite	3	FeTiO3
glass	25	Si0.98Al0.02Na0.008K0.002Ca0.002Fe0.001O2

In the model, it was speculated that a sequence of thin layers of igneous rocks had potential to store CO_2 and that a sedimentary layer was considered an appropriate seal zone for the following reasons:

1. Fractures in the igneous rocks indicated that tectonic activities caused deformation during the Jurassic era (Heffner, 2013). These fractures enhanced the permeability of the rock in places where tectonic forces were produced and changed the structure of the thin igneous layers. Sandstone layers, common sedimentary rock layers found in the SGR basin, are more tolerant of tectonic forces when compared to igneous rocks. This is because sedimentation occurred in the SGR basin after the previously described igneous rifting process during the Jurassic era. Consequently, the permeability of sedimentary layers were rarely affected by tectonic forces in comparison to igneous rocks.

2. The thickness of the sedimentary formations was believed to be 5 km, thicker than previous estimates, resulting in very low porosity and permeability values and making them suitable to serve as a CO_2 seal.

7. Results and discussion

Theoretically, values close to zero mD fault permeability are expected to show leakage that could be controlled. Small values of fault permeability (0.1, 0.15, 0.3, and 0.5 mD) and logarithmic values (1, 10, 100, and 1000 mD) were selected to investigate the relationship between fault permeability and CO_2 distribution in the CO_2 simulation models. The initial results demonstrated the following:

1. Permeability values close to zero (0.1, 0.15, 0.3, 0.5, and 1 mD) allowed for slow leakage of carbon dioxide in a critical range that could be stopped by mineralization (Figure 6).

In contrast, fault permeability that exceeded 1 mD provided limited control of carbon dioxide despite the wide range tested using the logarithmic scale (Figure 6). It is important to note that while the CO_2 migration was similar for a large range of fault permeability values between 10 and 1000, the small range tested at permeability values close to zero highlighted a critical variation in leakage control.

2. Both vertical migration of CO_2 and fault permeability were inversely proportional to seal resistancewhen take in an account that falut permeability values always larger than seal permeability (Figure 6).

In the simulations with low fault permeability values, we observed that the models with less than 10 mD reflect resistance against the migration of carbon dioxide and show minimum leakage (Figure 6). The resistance behavior clearly appeared between the reservoir zone D-E and the upper seal zone (SSTN-1). To allow for this resistance, the CO_2 plume was located at the upper layers of the reservoir zone due to supercritical and gaseous CO_2 having a smaller specific gravity than the formation water. This behavior was particularly associated with lower permeability values 0.1, 0.15, 0.3, and 1 mD. In contrast, the models that had a fault permeability greater than or equal to 10 mD showed the opposite behavior (Figure 6). When greater values were used, most of the CO_2 migrated to the D-C zone in the upper part of the model through the fault zone due to low resistance of the seal.

In the model, a fault that had a high permeability did not support mineralization because the CO_2 plume was distributed in a wide area behind the seal zone. However, for faults that had small permeabilities, chemical reactions that occurred between CO_2 and the basaltic rock were able to stop CO_2. In both scenarios there were two-time domains. The first one controlled the migration of the CO_2 plume and depended on permeability. The second time domain controlled the chemical reactions that allowed for the mineralization of the CO_2 plume after rapid dissolution (Gislason et al., 2014).

Assuming that mineralization would reduce the permeability or fractures of a fault within the seal zone, slowing the vertical migration of CO_2 was needed in the model to grant the second time domain an opportunity to mineralize CO_2 because the mineralization works is a slow process (Yuan et al., 2022). For example, the first case utilized critical permeability values for CO_2 mineralization as they enhanced the
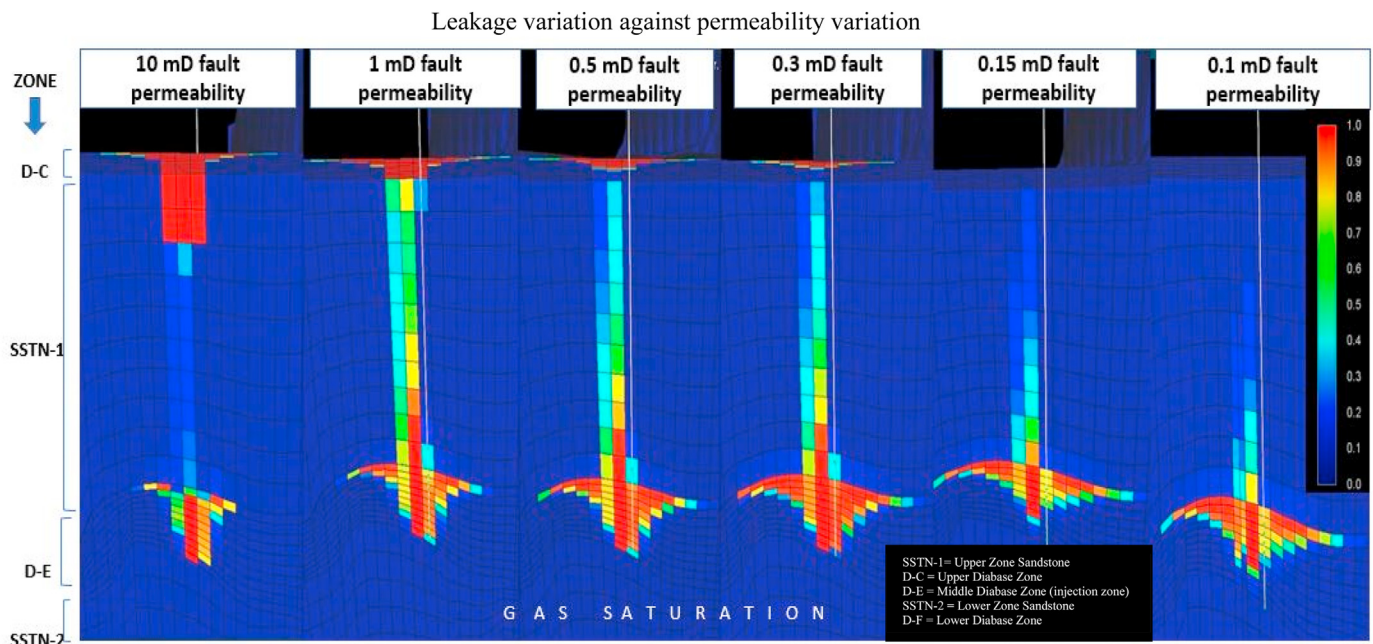
Figure 6. Display of selected models with respect to fault permeability at the end of the simulation time (year = 2100) in the case of no mineralization. Applying the simulation showed that resistance was inversely proportional to the fault permeability value. The higher fault permeability values showed a lower resistance to CO_2 migration. The gradient of color reflects the CO_2 saturation in the model. Models for higher values of permeability show that a part of the CO_2 plume rose to the top of the model as a result of low resistance of the seal zone SSTN-1. For the permeability of 0.1 mD, CO_2 almost failed to penetrate the upper seal. In contrast, permeabilities greater than or equal to 0.3 mD allowed CO_2 to pass the seal zone SSTN-1.

opportunity for CO_2 solid phase sequestration (Table 3). This is because mineralization requires keeping the injected CO_2 within the reservoir as much as possible in order to maintain the mineralization process, which was accomplished when using critical permeability values. On the contrary, carbon dioxide high leakage could reduce the concentration of the aqueous phase to a large scale and thus loses the efficiency thee mineralization process.

The time required for the CO_2 plume to reach the top of the simulation model (arrival at the D-C zone) was considered to be a function of fault permeability. The years that the carbon dioxide plume first appeared at the top of the model for fault permeability values of 10, 1, 0.5, 0.3, and 0.15 mD were 2025, 2037, 2052, 2067, and 2105, respectively (Table 3). An applied permeability of 0.1 mD showed that CO_2 could not migrate through the fault to the upper D-C zone until the simulation year 2116 (Figure 6, Table 3) due to the maximum resistance exhibited by the seal zone SSTN-1 against CO_2 migration. This case

identified that the minimum 0.1 mD limit of fault permeability did not allow for CO_2 to migrate to the upper zone. At a fault permeability of 0.1 mD, CO_2 barely penetrated several layers in the seal zone (SSTN-1) despite continuous CO_2 injection throughout the entire simulation (Figure 6). In contrast, a fault permeability of 10 mD showed that the CO_2 plume was split into two parts. In this case, the part that split from the original plume penetrated the seal SSTN-1 and was located at the top. This indicated low resistance, corresponding to higher permeability values. Some of the cases exhibited different behavior depending on the permeability of each zone. For example, in case 2 (Table 3, Figure 7), a continuous injection of CO_2 into zone D-E resulted in two patterns of aqueous CO_2 in the reservoir for fault permeabilities 0.1 mD and 1 mD. For both patterns of aqueous CO_2 distribution, the corresponding leakage exhibited between 2016 to 2030 increased in the injection zone D-E in an exponential manner. Additionally, the seal zone SSTN-1 resisted CO_2 movement so that from 2016 to 2100 the CO_2 was released at a constant rate. For a specific amount of CO_2 injected and various fault permeabilities, the behavior of the leakage was the same for these different zones but the magnitude of CO_2 leakage varied. The upper D-C zone was not affected by the CO_2 migration because the fault permeability value was small and prevented CO_2 migration vertically through the fault wall. The total amount of CO_2 in the aqueous phase in case 6 (0.1 mD permeability) was 6.4E+8 mol (Figure 7A). Case 2 (1 mD) exhibited more complex relationships when compared to Case 6. However, case 2's zones D-E and

Table 3. Six models have been applied in simulation against selected values of fault permeability and reflect a time sequence for first appearing at the top layer of the 3D model as an indicator of the speed of migration, the 10 mD F.p. In case 1, the migration time is fast to arrive at the top layer of (D-C) 2025 from the simulation start time in 2016 and graded as a weak resistance. While the value 0.1 in case 6 gave the maximum time that extended at the end of the simulation time in 2116 and graded as a Full resistance (No – Vertical Migration).

Case No.	Fault permeability (mD)	First, arrive at the top of the model	Resistance	Notes
1	10	2025	Weak	
2	1	2037	Low	
3	0.5	2052	medium	
4	0.3	2067	Good	
5	0.15	2105	Very Good	
6	0.1	———	Full	No indicator for immigration until end of the simulation

Table 4. Shows the reactive surface area against the minerals and the setting of the minerals species components. the reactive surface area is varying significantly on small scale (luo2012). The values were modified from laboratory testing from the computer modeling group.

Mineral reaction	Reactive surface area	Mol/m2s	J/mol	Deg C
Calcite	88	-8.79588	41870	30
Kaolinite	17600	-13	62760	30
Anorthite	88	-12	67830	30

Modified From (CO_2 sequestration using GEM 2016.1)
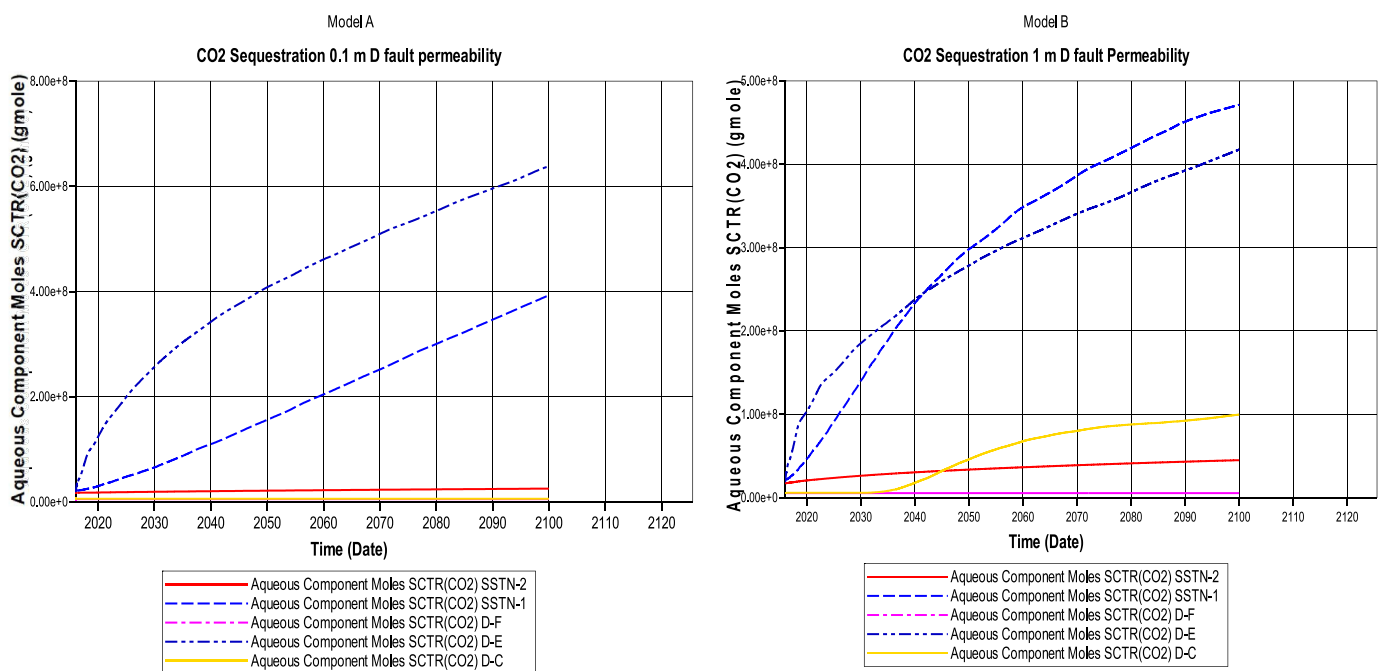
Figure 7. Pattern variations of CO_2 in the aqueous phase for two fault permeabilities with respect to time. At 0.1 mD, the variation of aqueous CO_2 in the injection zone leaked at a constant rate and reflected the higher resistance of seal zone SSTN-. The upper zone D-C was not affected as a result of the effective seal which controlled the CO_2. For 1 mD, there was a variation in aqueous phase CO_2 at year 2036 in the top zone which showed evidence of minor leakage due to the low resistance to CO_2 migration within the upper seal SSTN-1.
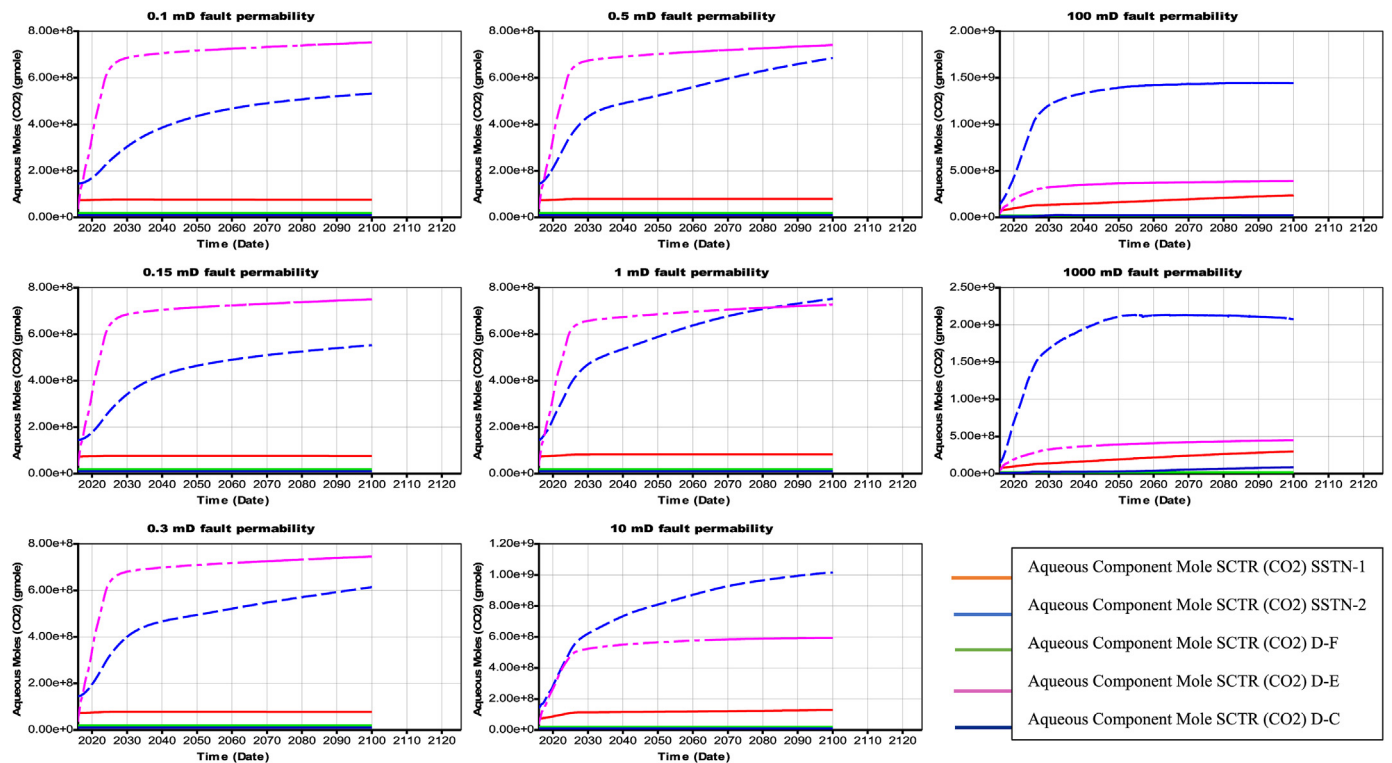
Figure 8. Aqueous phase CO_2 presence over time in all model zones for various permeabilities. The CO_2 plume migration varied in each zone depending on fault permeabilities ranging between 0.1-1000 mD.
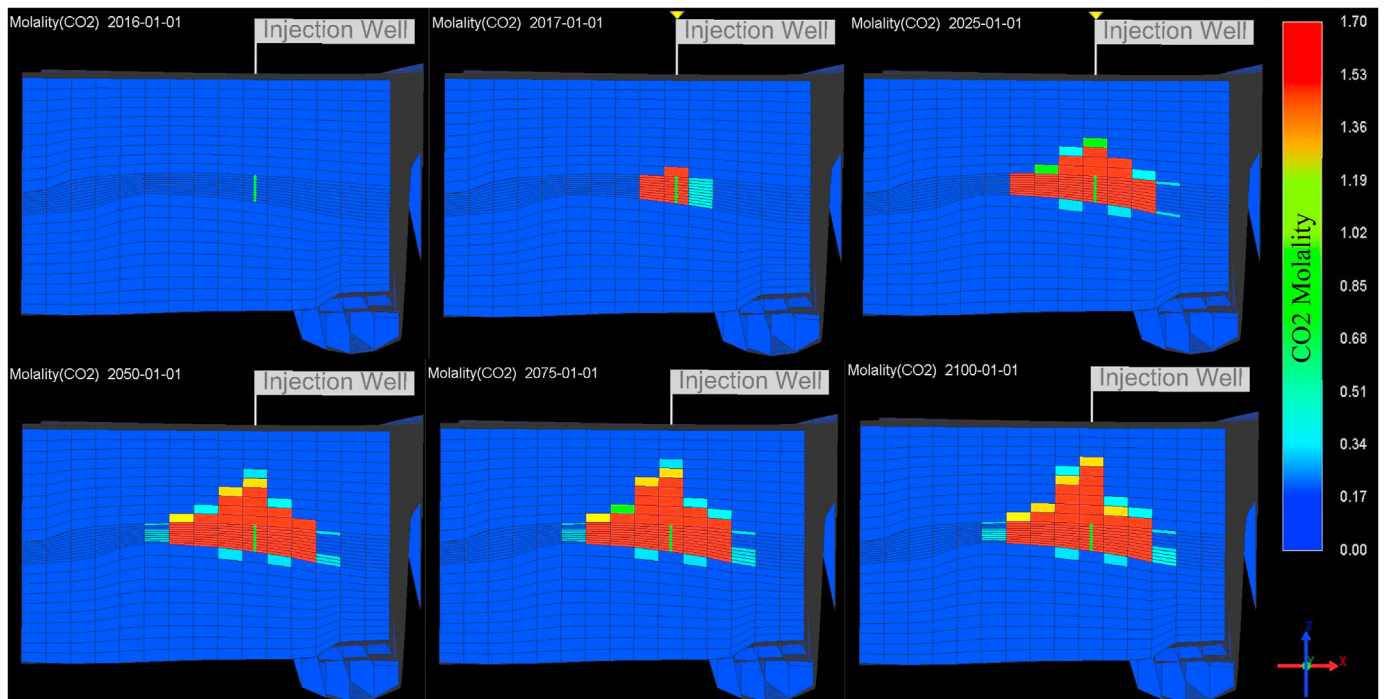

Figure 9. Mechanism of CO_2 plume migration around the injection well. In the short time between the beginning of injection in 2016 to the end of injection in 2036, the distribution of CO_2 increased rapidly due to the high permeability of the injection zone and then slowed after injection finished. During injection, CO_2 spread horizontally but after the injection stopped, CO_2 spread vertically into other zones. The permeability in the fault zone for this model was constant at 1 mD.

SSTN-1 exhibited the same pattern. In case 2, the aqueous phase first arrived at the D-C zone in the year 2035, and the CO_2 concentration was 1E+8 mol at the end of the simulation year 2100 (Figure 7B). This highlighted the relationship between decreasing amounts of the CO_2 plume in the injection zone D-E that was limited by fault permeability. In addition, it highlighted the corresponding first arrival and amount of the plume in the upper D-C zone. The lower seal (SSTN-2) controlled migration for aqueous CO_2, which was expected due to the increasing injection pressure with time and the smaller specific gravity of CO_2 when compared with the formation water. This moved the aqueous CO_2 to several layers of SSTN-2, but that effect did not extend to the lower zone (D-F). In the case that there was no mineralization, this work recognizes that the CO_2 plume varied in both the reservoir, seals, and upper zone and that fault permeability was proportional to the time to first arrival of the plume at the top of the model.

When mineralization was simulated in this model, it demonstrated supercritical CO_2 injection within the reservoir D-E between two seal zones SSTN-1 (top) and SSTN-2 (bottom). During this process, a chemical reaction was expected to occur between the CO_2 and igneous rocks in the injection zone starting immediately when CO_2 mixed with formation water to dissolution occurs (Gislason et al., 2014). The chemical reactions that lead to mineralization were adjusted by WINPROP software, a part of the CMG package 2107 software, which considered the chemical parameters in Table 4 according to Eqs. (1), (2), (3), (4), (5), and (6).

Calcite distribution for the logarithmic scale
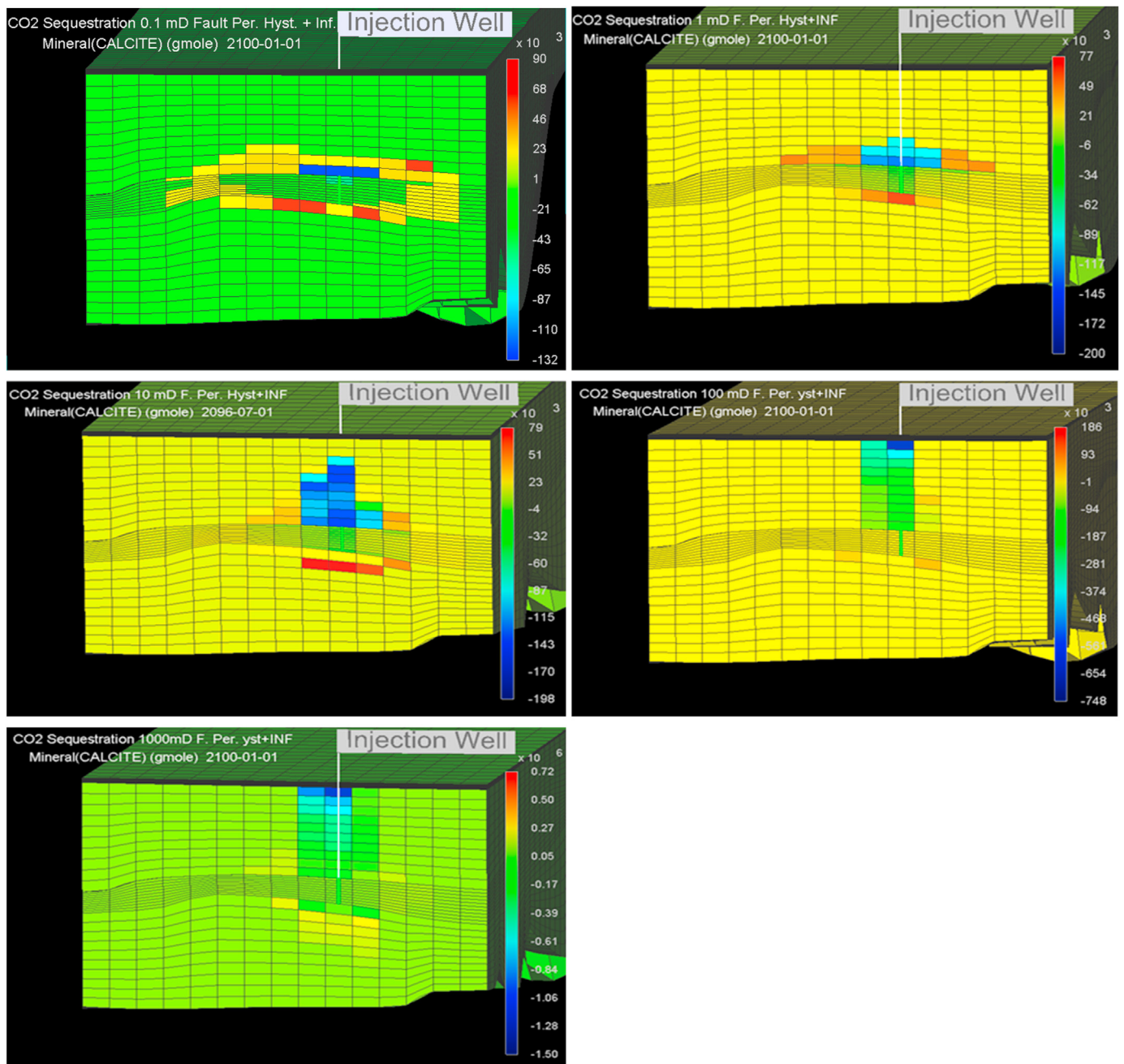
Figure 10. Impact of fault permeability on calcite distribution. This figure shows calcite distribution for the logarithmic scale of permeability and highlights the associated migration patterns. For the wide range of permeability values applied the results were polarized as only widespread leakage or no leakage was observed. Although mineralization occurred, it is difficult to control the plume migration.

In the model, supercritical CO_2 first dissolved into a formation's water around the injection well within injection zone (D-E) and formed carbonic acid, H^+ and, HCO_3^- (Eqs. (1) and (2)). At that point, CO_2 in the aqueous phase began to distribute rapidly according to the permeability of the injection zone (Figure 8). Throughout the injection, the amount of H^+ and HCO_3 continued to increase (Law and Bachu, 1996).

After the injection, H^+ and HCO_3^- started to react with the igneous rock to release a second group of ions including Mg, Fe, and Ca. In tandem, the igneous rocks also reacted with H^+ and HCO_3 from Eqs. (1) and (2) to form carbonate rock, as described in Eqs. (3) and (4). For example, Forsterite reacted with ions from Eqs. (1) and (2) to produce $MgCO_3$ which is more stable than forsterite. Similarly, calcite, kaolinite, and
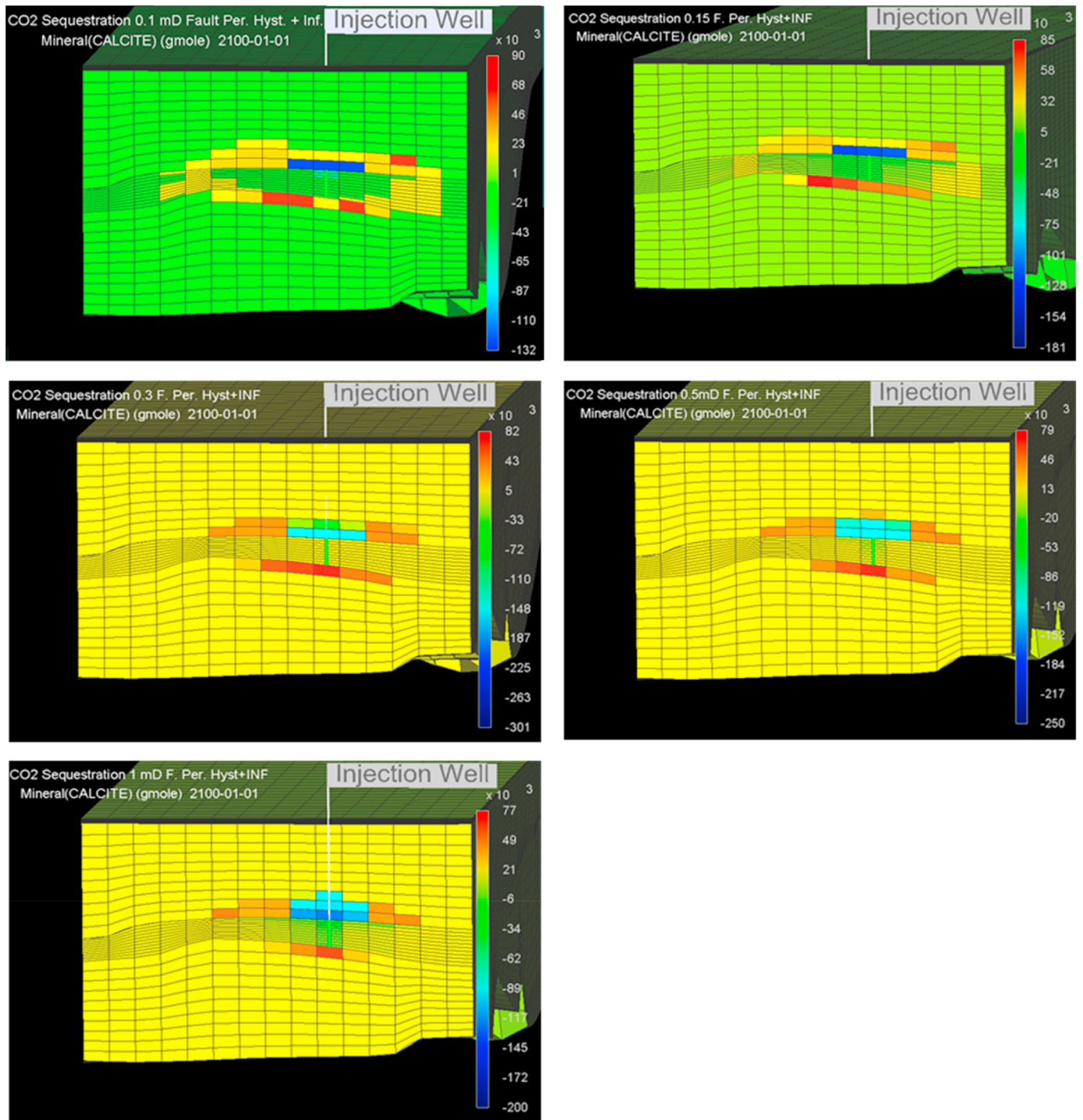
Figure 11. Effects of changing fault permeability on the distribution of the CO_2 plume. When the permeability was small, the resistance of the seal forced the migration to be slow and the carbonite rock production in proximity to the leakage reduced vertical migration. Increasing the cumulative pressure at the bottom seal reduced the vertical migration for the CO_2 plume.

Anorthite distribution for the logarithmic and critical scale

Figure 12. Anorthite dissolution with respect to fault permeability. At a low fault permeability values, horizontal migration occurred. Higher fault permeability values corresponded to vertical migration of the CO_2 plume.

magnesite were also by products that resulted from cumulatively increasing the concentration of Mg and Ca ions in the aqueous phase (Eqs. (4), (5), and (6)). After the completion of the c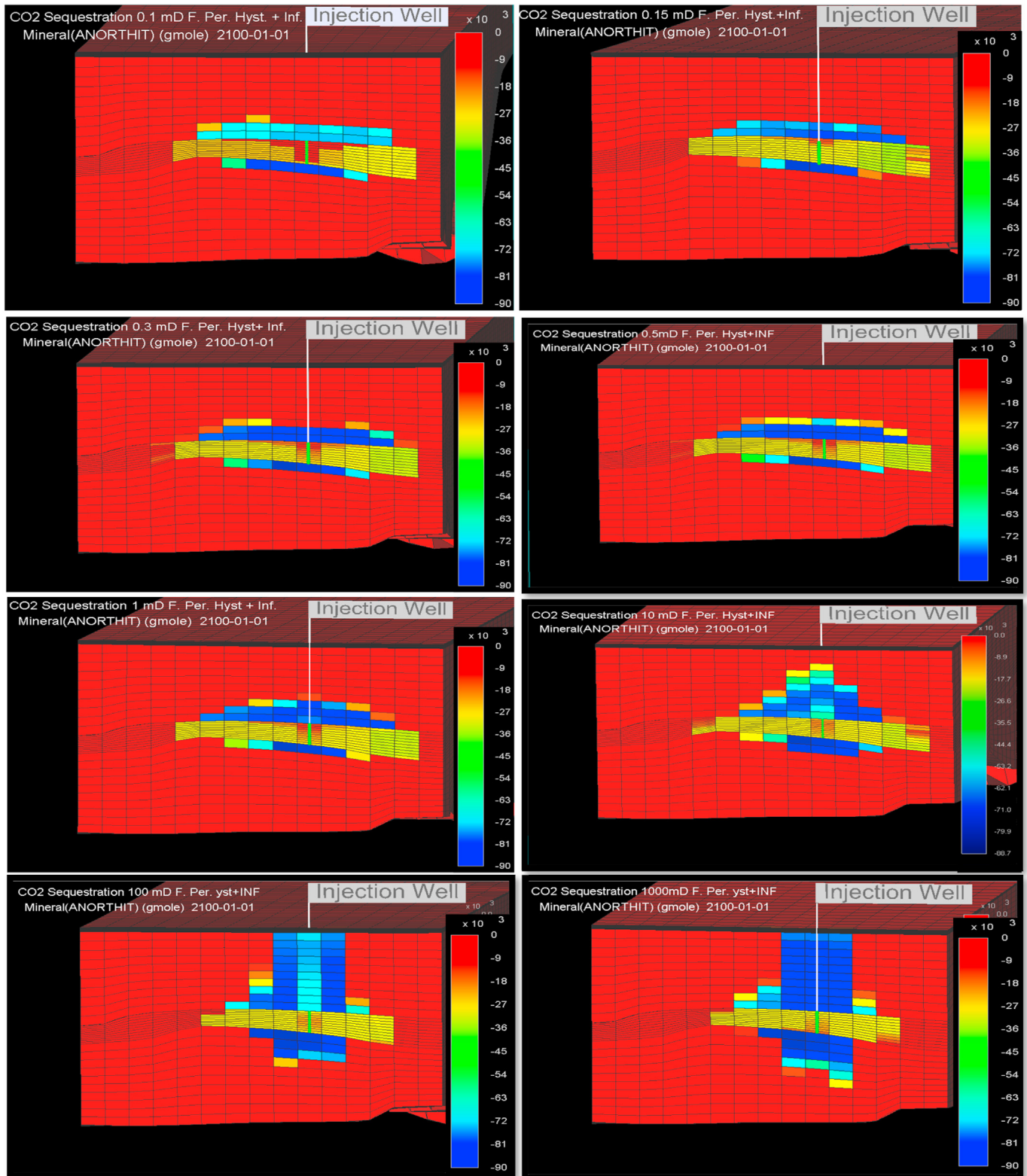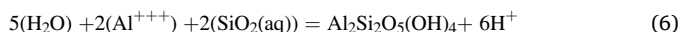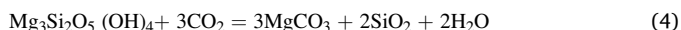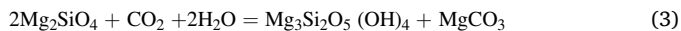hemical reactions described in Eqs. (1), (2), (3), (4), (5), and (6), it was difficult to predict if all potential carbonate rocks formed for the determined simulation period of 200 years (Aradó ttir et al., 2011).

Equations:

$$CO_2 (g) + H_2O \leftrightarrow H_2CO_3^- \tag{1}$$

$$H_2CO_3 \leftrightarrow (H^+) + (HCO_3^-) \tag{2}$$

$$2Mg_2SiO_4 + CO_2 + 2H_2O = Mg_3Si_2O_5 (OH)_4 + MgCO_3 \tag{3}$$

$$Mg_3Si_2O_5 (OH)_4 + 3CO_2 = 3MgCO_3 + 2SiO_2 + 2H_2O \tag{4}$$

$$(Ca^{++}) + (HCO_3^-) = CaCO_3 + H^+ \tag{5}$$

$$5(H_2O) + 2(Al^{+++}) + 2(SiO_2(aq)) = Al_2Si_2O_5(OH)_4 + 6H^+ \tag{6}$$

In the model, the chemical reactions depicted in Eqs. (3), (4), (5), and (6) occurred slowly due to several factors that affected mineralization. The carbonic acid involved in mineralization is a weak acid which caused slow chemical reactions (Khan et al., 2015). In addition, the 20 year injection period of CO_2 limited the amount of CO_2 available for mineralization, causing a slower process. In addition, because the model was a partially open system, part of the CO_2 plume migrated through the fault before mineralization could occur which reduced the efficiency of mineralization in the reservoir and seal.

Modeling a 20 yearlong injection of 10 M m³/year of supercritical CO_2 for critical and logarithmic values of fault permeability and the subsequent 200 years showed important results. The key findings concerning solubility processes, mineralization patterns, and kinetic reactions are described below.

7.1. Solubility processes

Solubility processes were observed when CO_2 was injected at a minimum depth of 2 km under expected increasing pressure and constant temperature. After the creation of carbonic acid and dissolution of CO_2 in the aqueous phase, H^+ and $HCO3^-$ extracted various cations including Ca, Fe, Mg, Si, and Al from igneous minerals (Figures 8 and 9). Depending on the CO_2 plume's propagation and buoyancy, the high porosity and permeability of the SGR basin's igneous rock supported the migration of the plume and caused it to move into the upper layers of the injection zone. The plume then attempted to penetrate the bottom layers of the seal (SSTN1). Due to the permeability of the fault zone in the seal, the CO_2 plume was able to move into the upper layers through the fault zone, the weakest area in the seal. The fault's permeability, in this case, was the controlling factor for mineralization (Figures 10 and 11). In other words, whenever the permeability was low, the leakage of the CO_2 plume moved slowly which allowed it to generate and deposit more carbonate minerals in a specific area.

In Figures 10 and 11, the effect of permeability on mineralization considering two scales of permeability is displayed. The logarithmic scale scenario, the models displayed in Figure 10 showed the CO_2 plume migration after mineralization of the carbonate rocks for models with 100 mD and 1000 mD. The CO_2 plume went into the atmosphere around 100 years of simulation. Due to low resistance related to high fault permeability, the CO_2 plume migrated a farther distance than that which corresponded to low permeability values. Consequently, mineralization did not take place in the fault area within the seal zone and did not produce carbonate rocks. Thus, the carbonate minerals created by mineralization passed the seal and were located in the upper part of the model. In contrast, the opposite was seen in the case of 0.1 mD and 1.0 mD fault permeability models. In these scenarios, the plume barely

Mineralization change variation of Anorthite
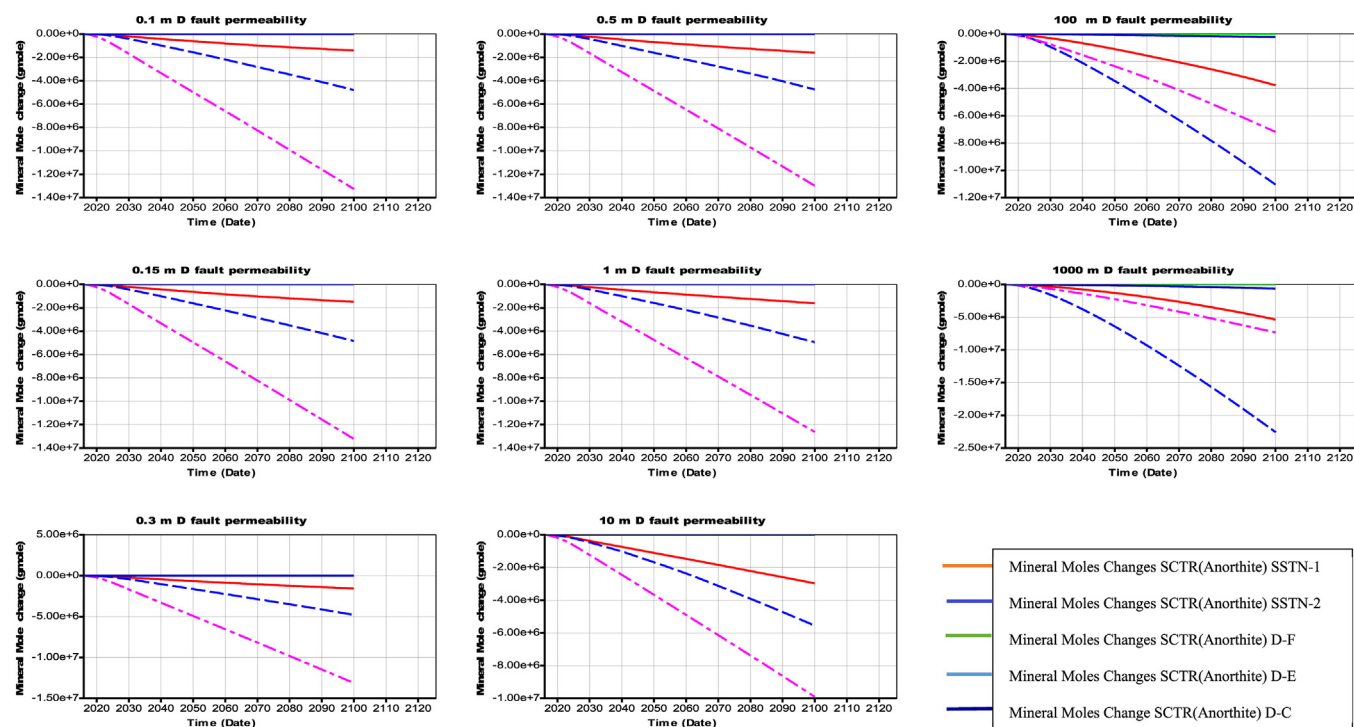
Figure 13. Dissolution of anorthite in various model zones with respect to fault permeability. While the dissolution rate varied, the dissolution of anorthite occurred for all permeability values and dissolved anorthite migration was inversely proportional to the resistance of the seal zone. The upper zone (D–C) was not affected in cases of low permeability as the CO_2 plume remained within the seal zone, which allowed for mineralization to occur. High values of fault permeability allowed the plume to move up without being affected by mineralization.

penetrated two or three bottom layers of the seal zone, and that forced the CO_2 plume to migrate downward vertically where pressure was higher due to the cumulative weight of rock and the pressure of injection. Consequently, the mineralization took place in the lower parts of the seal and around the injection zone.

The most complicated case found in this study was the model that used a 10 mD fault permeability. Even though this value of permeability offered adequate time for mineralization (the same or a similar time required for 0.1 and 1 mD when compared to 100 and 1000 mD), the plume moved through the seal zone to relocate close to the top layers of the SSTN1 seal zone. Consequently, it was undecided whether or not the CO_2 plume escaped into the atmosphere. If the simulation time was extended 100 years, more details could be seen regarding the fate of the CO_2 for the 10 mD fault permeability model. In this case, the logarithmic scale was not accurate enough and failed to predict the effect of fault permeability on CO_2 plume migration. This is important because previous studies that used the logarithmic scale determined that the CO_2 plume escaped to the atmosphere in all non-zero permeability cases (Brantley et al., 2015).

Identifying the critical range of fault permeability (0.1–1 mD) that was needed to build a mineralization model was the prime focus of this study despite of increasing reactive surface area could be higher in light fault permeability values (Luo et al., 2012). By using this limit of critical permeability in simulation, The mineralization efficiency has been enhanced and becomes able to reduce the risk of leakage from small values of permeabilities. The simulation results showed that an effective seal was created through mineralization by transferring minerals from the injection zone to the seal zone. Mineralization likely helped repair the seal by inhibiting leakage and decreasing the permeability of the seal zone. The migration time domain was considered to be a function of permeability and used to describe changes in permeability in a heterogeneous model where mineralization was applied. When comparing the first arrival of CO_2 at the top of the model in Figures 6 and 11, both figures had the same permeability values but only Figure 11 included mineralization which limited CO_2 migration. This indicated that mineralization reduced the permeability of the fault seal. Applying mineralization also resulted in more storage capacity being added to the original volume that was calculated using porosity and permeability in the injection zone. Aqueous CO_2 supported the migration of ions described in Eqs. (1), (2), (3), (4), (5), and (6) from the injection zone to the target location within the fault area in the seal zone (Figure 11).

The advantage of fault permeabilities on the logarithmic scale was the increased potential of mineralization due to the greater volume in the fault. However, the disadvantage to permeabilities this size was that the areas of solubility extended to the upper zone of the model and inhibited leakage mitigation. By using this limit of critical permeability in simulation, a method was found to reduce the risk of leakage from small values of permeabilities.

7.1.1. Solubility of anorthite

Anorthite is a common mineral found in igneous rocks. It is considered an abundant cation source and is able to react with carbonic acid to form aqueous phase CO_2 after injection. While anorthite provided a fast dissolution rate in the injection zone (D-E) at the beginning of the simulation in all permeability values (Figure 9) (Figure 12), the CO_2 plume vertical migration moved at different rates depending on the fault permeability. In the case of low fault permeability (0.1–1 mD), the aqueous phase barely penetrated several layers of the bottom part of the upper seal (SSTN-1) despite a higher carbonic acid concentration. Due to the low permeability, carbonic acid had a maximum ability to react with minerals only near the injection zone.

In the model, the concentration of carbonic minerals was higher at the edge of the aqueous phase of the CO_2 plume in comparison to the center (Figure 8 and Figure 13). With higher fault permeability values, the dissolution of CO_2 continued through both seals SSTN-1 and SSTN-2. The difference between the CO_2 plume's time to arrival at the top of the model

was dependent on the propagation of the buoyant supercritical CO_2. The amount of anorthite that was dissolved in the upper seal was higher than that in the injection zone (D-E) and was comparable among all models that showed some CO_2 between the upper seal and bottom seal (Figure 14). This study focused more on the upper seal zone (SSTN-1) because it had a greater risk for leakage into the atmosphere in comparison to the bottom seal (SSTN-2).

Table 5. shows the relationship in every zone between calcite reaction behavior and fault permeability. The calcite has two main patterns, the dissolution in the first stage then conversion to deposition in the second stage. Reduction of the permeability will enhance the ability to dissolve in the injection zone and vice versa in the seal zone. The other igneous zones (D-C and D-F) were not affected by fault variation except the (100 and 100 mD) in top zone as the indicator of no resistance against CO2 migration.

NO	Zone	F.Perm.	Max dissolution value	Equilibrium	Deposition gmole
1	D-C	1000	(-)0.424 EXP 06	non	0.839 EXP 06
2	D-C	100	(-)0.329 EXP 06	non	0
3	D-C	10	0	non	0
4	D-C	1	0	non	0
5	D-C	0.5	0	non	0
6	D-C	0.3	0	non	0
7	D-C	0.15	0	non	0
8	D-C	0.1	0	non	0
1	SSTN-1	1000	(-)2.26 EXP 07 at 2051	0	2.855 EXP 07
2	SSTN-1	100	(-)1.19 EXP 07 at 2041	0	9.602 EXP 06
3	SSTN-1	10	(-)5.63 EXP 06 at 2060	0	5.337 EXP 06
4	SSTN-1	1	(-)3.042 EXP 06 at 2043	0	6.267 EXP 06
5	SSTN-1	0.5	(-)2.92 EXP 06 at 2036	0	6.311 EXP 06
6	SSTN-1	0.3	(-)2.6 EXP 06 at 2036	non	6.809 EXP 06
7	SSTN-1	0.15	(-)2.25 EXP 06 at 2036	0 at 2096	7.388 EXP 06
8	SSTN-1	0.1	(-)2.014 EXP 06 at 2036	0 at 2090	7.953 EXP 06
1	D-E	1000	(-)3.071 EXP 06 at 2030	0 at 2074	1.530 EXP 07
2	D-E	100	(-) 3.026 EXP 06 2026	0 at 2070	1.557 EXP 07
3	D-E	10	(-) 4.79 EXP 6 at 2026	0 at 2069.7	1.883 EXP 07
4	D-E	1	(-) 5.75 EXP 06 at 2026	0 at 2066.7	2.336 EXP 07
5	D-E	0.5	(-) 5.88 EXP 06	0 at 2066.5	2.405 EXP 07
6	D-E	0.3	(-) 5.9 EXP 06	0 at 2066.8	2.429 EXP 07
7	D-E	0.15	(-) 5.93 EXP 06	0 at 2066.5	2.451 EXP 07
8	D-E	0.1	(-) 5.93 EXP 06	0 at 2066.7	2.450 EXP 07
1	SSTN-2	1000	(-)0.762 EXP 06	0 at 2054	2.288 EXP 07
2	SSTN-2	100	(-)0.732 EXP 06 at 2026	0 at 2059	1.289 EXP 07
3	SSTN-2	10	(-)0.64EXP 06 at 2025	0 at 2045	6.335 EXP 06
4	SSTN-2	1	(-)0.164 EXP 06 at 2024	0 at 2033	3.450 EXP 06
5	SSTN-2	0.5	(-)0.1 EXP 2024	0 at 2029	3.289 EXP 06
6	SSTN-2	0.3	(-)0.061 EXP 2024	0 at 2028	3.092 EXP 06
7	SSTN-2	0.15	(-)0.036 EXP 06	0 at 2027	2.850 EXP 06
8	SSTN-2	0.1	(-)0.04 EXP 2020	0 at 2027	2.357 EXP 06
1 to 8	D-F	All	0	non	0

7.2. Mineralization patterns

7.2.1. Mineralization of calcite

Calcite is one of the stable carbonate minerals that is produced from the chemical reaction between anorthite and carbonic acid. The mechanism of the calcite mineralization can be clarified by simplifying the distribution of calcite in every zone and is described in Table 5. In the injection zone D-E, calcite showed the following patterns:

(1) Dissolution started at the beginning of the simulation in 2016 and arrived at the maximum value in 2026. H+ and HCO3- ions generated through dissolution during this time allowed the aqueous CO_2 to react with basalt and deposit calcite at the end of the chemical reaction series (Figure 14). Applying the maximum value of fault permeability to the model resulted in a minimum value of dissolution and vice versa for a low value of fault permeability. This is because greater permeabilities increased the probability that the CO_2 plume could rise up more quickly and cause leakage. In contrast, low values of fault permeability kept the supercritical CO_2 trapped in the injection zone. Consequently, more time was allowed for the reactions that dissolved anorthite and calcite in the injection zone (D-E).
(2) The equilibrium point between dissolution and mineralization was typically 50 years after the starting point of the simulation in 2016. Reducing the amount of calcite dissolution caused a delay in the time to the equilibrium point (Table 5).
(3) The precipitation rate of calcite minerals was inversely proportional to the fault permeability. With the high concentration of Ca^{++} cations, more calcite was deposited over time, especially at the end of the simulation in year 2216.

The upper seal (SSTN-1) showed that calcite dissolution was proportional to fault permeability with no equilibrium point except at fault permeability values of 0.1 and 0.15 mD. These low permeability values generated equilibrium points at years 2090 and 2096,

respectively. These values also produced 7.953 E06 and 7.388 E06 g mole of calcite, respectively. In cases where equilibrium was not reached, the upper seal zone was similar to an open system that allowed CO_2 to escape into the atmosphere. This allowed the CO_2 plume to move up and prevented equilibrium, especially for fault permeability values greater than 0.15 mD. If CO_2 migrated to the top of the model (D-C), it was considered to have escaped to the atmosphere. In case that the CO_2 reached this zone, the system failed to sequester CO_2. This occurred for fault permeability values 100 and 1000 mD where calcite dissolution of 0.329 E06 and 0.424 E06 g mole, respectively, was detected at the top of the model. Other fault permeability values did not show any dissolution in that location, indicating efficient calcite mineralization (Table 5).

Zone D-F did not show any mineralization or dissolution activities unlike that observed in zone (D-C). However, in the bottom seal (SSTN-2), dissolution or mineralization was detected. In contrast to the upper seal, the bottom seal's dissolution was proportional to fault permeability and better reflected equilibrium. The bottom seal's higher permeability delayed equilibrium because a higher pressure with depth enhanced the model's solubility during injection time. However, after the 20 year injection period, the bottom seal's behavior changed. As the injection pressure was reduced, it allowed for calcite mineralization between 100 and 1000 mD which was comparable to mineralization rates that occur at higher values of permeability (Tab-6). Overall, calcite mineralization was proportional to permeability in both seal zones. However, the CO_2 plume arrived at the equilibrium point in SSTN-2 (lower seal) earlier than in the SSTN-1 zone (upper seal).

7.2.2. Kaolinite

Kaolinite is a clay mineral that is produced from the reactions between H_2O, CO_2, and anorthite. Kaolinite mineralization was observed for all values of applied fault permeabilities (Figure 15 and Table 6). In the injection zone (D-E), kaolinite mineralization was inversely proportional to fault permeability. In the seal zones (SSTN-1 and SSTN-2), kaolinite mineralization was proportional to the fault permeability.
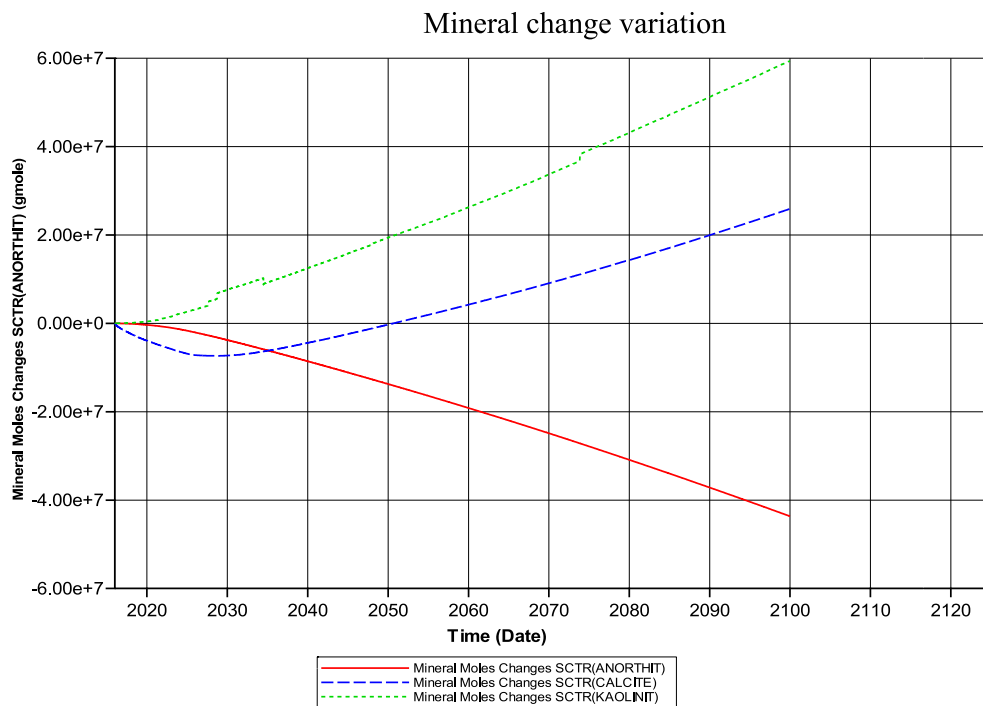
Figure 14. The chemical processes of anorthite, calcite, and kaolinite throughout the simulation. At the beginning of injection in 2016, calcite began to be dissolved, which increased until 2036. After the injection finished, calcite arrived at its maximum saturation point and it began to mineralize which lasted until the end of the simulation time in 2100. Throughout the simulation, anorthite dissolved constantly against the deposition of kaolinite.

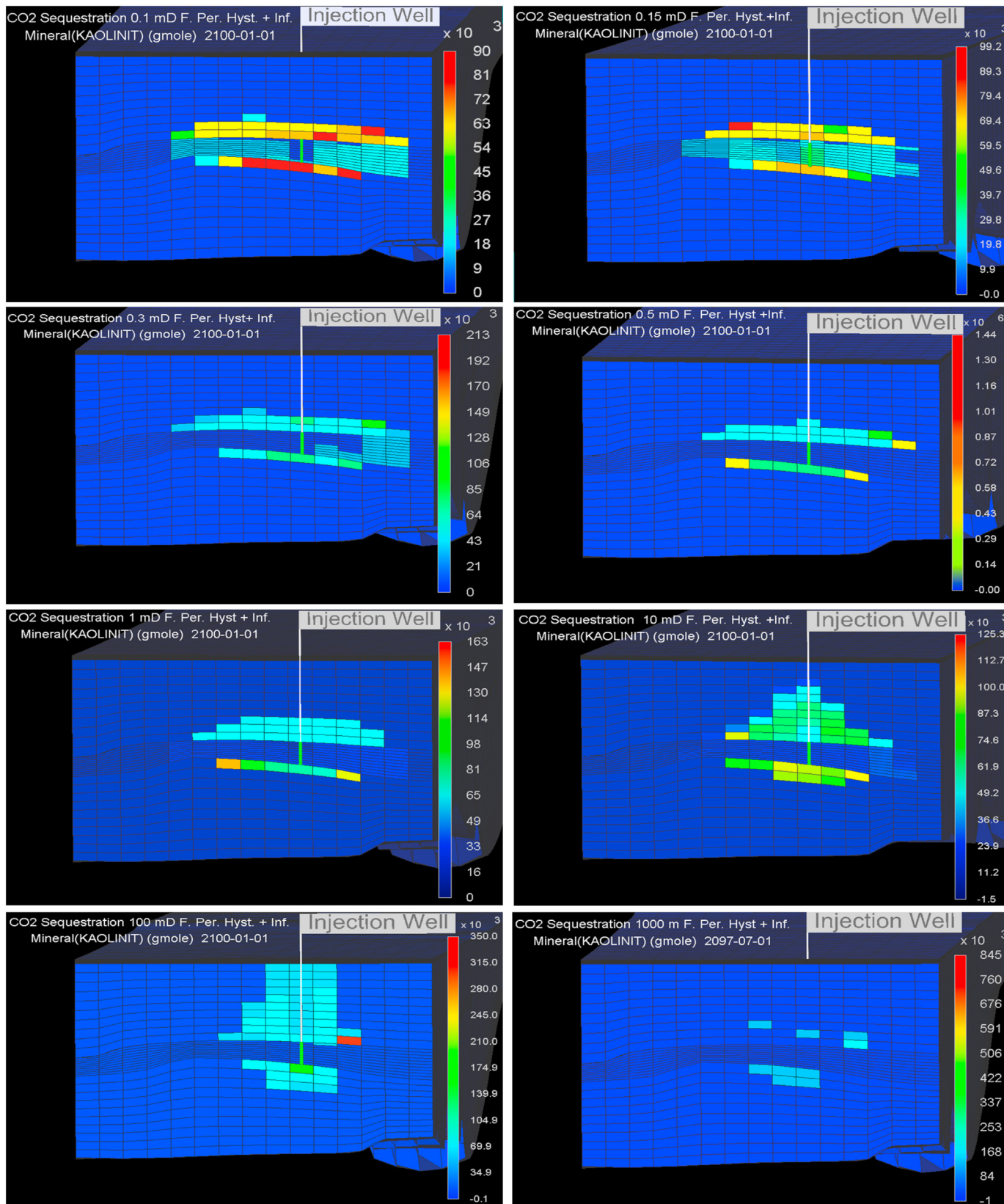# Kaolinite distribution for the logarithmic and critical scale

Figure 15. Kaolinite mineralization with respect to fault permeability. This figure shows that kaolinite mineralization occurred at all permeability values.

Table 6. The relationship between Kaolinite behavior and fault permeability in each zone. In general, there is a depositional situation in all zones at different ratios. The mineralization appears clearly in the case of reduction in the fault permeability in the injection zone (D-E) and top seal (SSTN-1). In contrast, the mineralization reduces when the fault permeability goes down. This implies that kaolinite prefers mineralization in the injection zone and above.

NO	Zone	F.Perm.	Dissolution	Equilibrium	Deposition gmole
1	D-C	1000	non	non	2.368 EXP 06
2	D-C	100	non	non	0.5905 EXP 06
3	D-C	10	non	non	0
4	D-C	1	non	non	0
5	D-C	0.5	non	non	0
6	D-C	0.3	non	non	0
7	D-C	0.15	non	non	0
8	D-C	0.1	non	non	0
1	SSTN-1	1000	non	non	7.238 EXP 07
2	SSTN-1	100	non	non	3.510 EXP 07
3	SSTN-1	10	non	non	1.705 EXP 07
4	SSTN-1	1	non	non	1.558 EXP 07
5	SSTN-1	0.5	non	non	1.607 EXP 07
6	SSTN-1	0.3	non	non	1.579 EXP 07
7	SSTN-1	0.15	non	non	1.540 EXP 07
8	SSTN-1	0.1	non	non	1.528 EXP 07
1	D-E	1000	non	non	2.131 EXP 07
2	D-E	100	non	non	2.027 EXP 07
3	D-E	10	non	non	2.545 EXP 07
4	D-E	1	non	non	3.193 EXP 07
5	D-E	0.5	non	non	3.287 EXP 07
6	D-E	0.3	non	non	3.367 EXP 07
7	D-E	0.15	non	non	3.377 EXP 07
8	D-E	0.1	non	non	3.395 EXP 07
1	SSTN-2	1000	non	non	2.293 EXP 07
2	SSTN-2	100	non	non	1.438 EXP 07
3	SSTN-2	10	non	non	8.557 EXP 06
4	SSTN-2	1	non	non	4.702 EXP 06
5	SSTN-2	0.5	non	non	3.394 EXP 07
6	SSTN-2	0.3	non	non	4.206 EXP 06
7	SSTN-2	0.15	non	non	4.059 EXP 06
8	SSTN-2	0.1	non	non	3.650 EXP 06
1 to 8	D-F	All	0	non	0

Kaolinite mineralization did not occur in the top (D-C) or bottom zone (D-F) except for fault permeabilities of 100 and 1000 mD, which showed some mineralization (0.590 E06 and 2.368 E06 g mole kaolinite, respectively) in the top zone (Table 6).
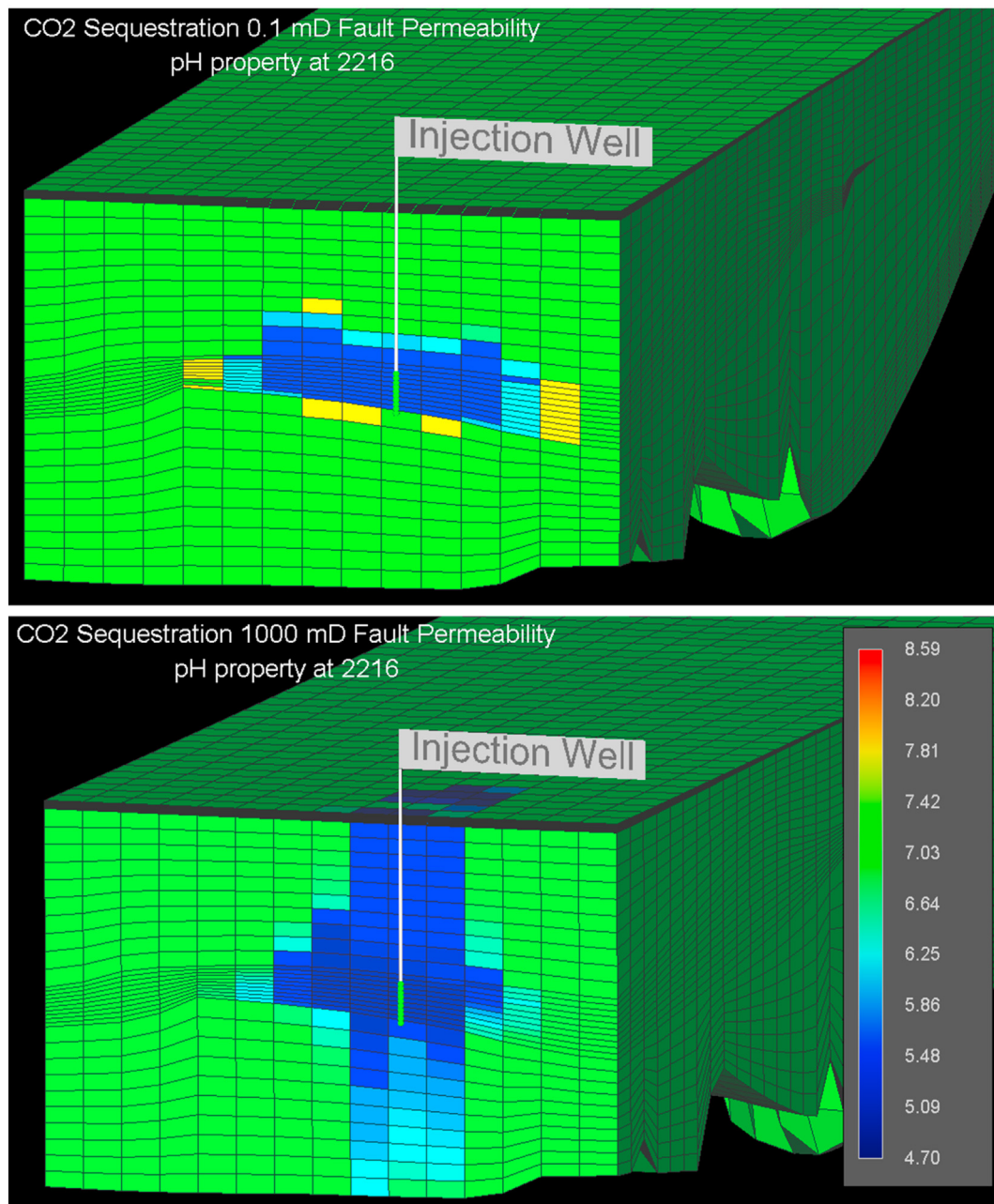
Some numerical calculations that were used to determine the amount of trapped CO_2 with respect to phase are shown in Table 7. Supercritical CO_2 was the initial phase of CO_2 injected into the formation and the amount in the formation after the injection period was inversely proportional to the fault permeability. A second phase was comprised of dissolved CO_2 in H_2O. The amount of the dissolved CO_2 in the formation after the injection period was proportional to fault permeability.

A third phase that existed in the model was aqueous CO_2 which was chemically dependent on cations in the formation water and inversely proportional to fault permeability. in the onshore injection the formation water tend to be low salinity. thus, the opportunely in storage CO_2 could be increased (EA Al-Khdheeawi et al., 2018). The final phase of CO_2 in the model was the solid phase created through mineralization and showed a variation of trends with different values of permeability. Notably, solid phase CO_2 observed at the end of the injection period was proportional to small values of permeability (0.1,0.15 mD) and inversely proportional to permeability values of 0.4,1, and 10 mD. It was then proportional again at values 100 and 1000 mD, but at the end of the injection, the carbonate minerals were not contained and escaped the seal zone.

7.3. Kinetic reactions

Contrary to what was found in the Rizer #1 borehole, it was assumed in the model that there was sufficient basaltic rock and formation water available so that these factors were not limiting for mineralization. Because no information could be found to support volcanic activities in the SGR Basin, temperature variation was assumed to be negligible and a constant temperature was used. The rate of a chemical reaction varied depending on permeability since there was a limited and constant injection rate of 10 million m^3/year of supercritical CO_2. At the beginning of the injection, the supercritical CO_2 mixed with the formation's water and formed the previously described dissolved phase. Meanwhile, the supercritical CO_2 in the formation continued to increase during injection to a maximum value of 2.27 E09 mole at 2036. During the injection period, the pH increased rapidly as indicated in Figure 16. Then, the amount of supercritical CO_2 in the formation decreased and was impacted by fault permeability, especially in the seal zones (Figure 17). The dissolution of supercritical CO_2 doubled between fault permeability 0.1 and 1000 mD, dissolving 1.5 E09 moles and 3 E09 moles of CO_2, respectively. The maximum dissolution value with respect to time in each zone illustrated that permeability impacted the CO_2 plume's migration (Table 5). Following the dissolution of CO_2, in the chemical reactions described in Eqs. (1), (2), (3), (4), (5), and (6) the solubility of CO_2 increased and was proportional to permeability in every zone except the injection zone. In the injection zone, fault permeability was inversely proportional to dissolution due to the horizontal movement of CO_2 related to the seals' high resistance (Table 5). In Eqs. (1), (2), (3), (4), (5), and (6), the reaction between the H^+ and HCO_3 and the

Table 7. The effects of fault permeability on CO_2 phase distribution. Despite the increasing presence of minerals with permeability, the migration of CO_2 phases did not allow mineralization in a suitable location. This shows that the mechanism of migration must be compatible with mineralization to locate the carbonite mineral in the appropriate location.

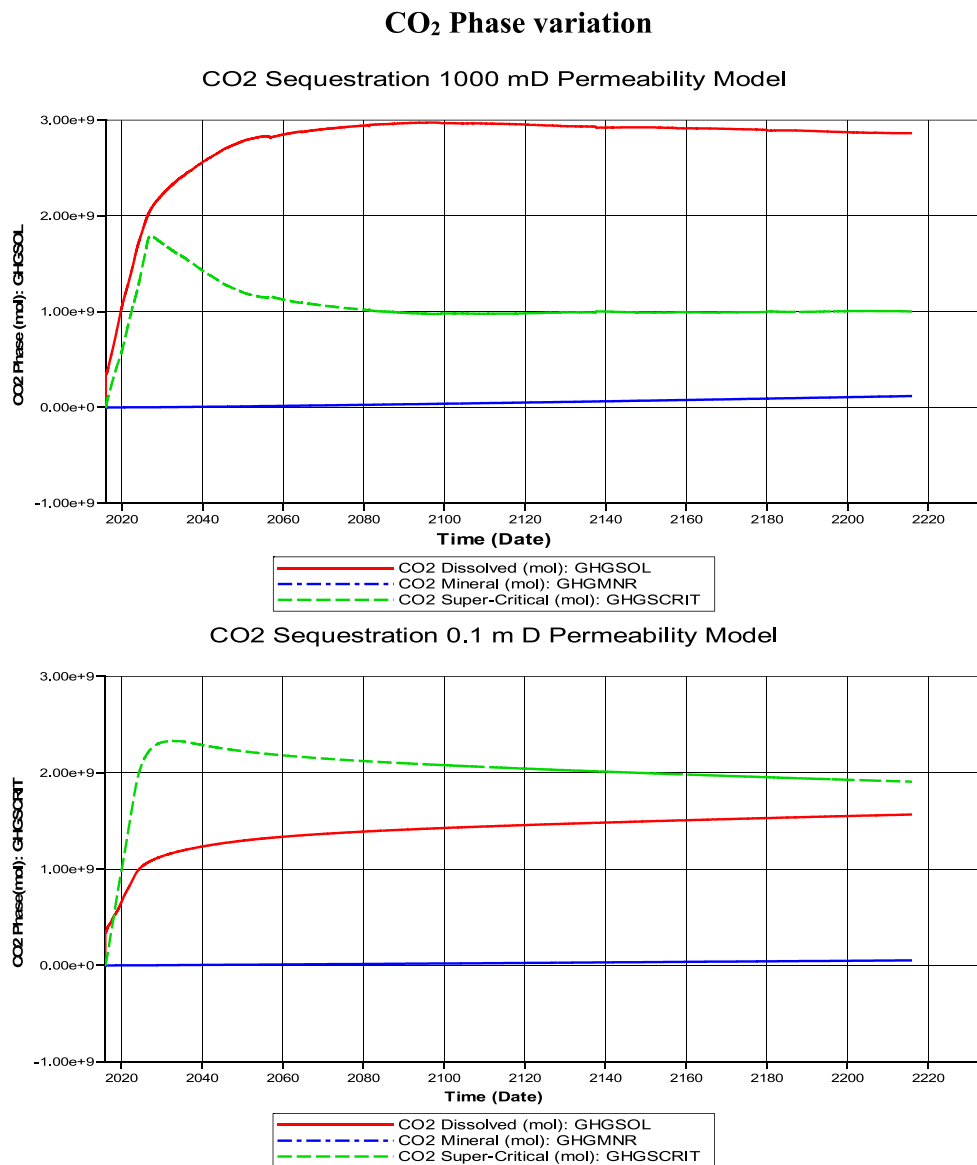| no	F.P. mD	Gaseous phase	Liquid Phase	Super critical Phase	Trapped/Hysteresis	Dissolve in water	Present in Aqueous Ions	Present im Mineral precipitate
1	0.1	0	0	2.01812 E+08	1.07701 E+08	1.38489 E+08	1.12164 E05	2.03615 E+06
2	0.15	0	0	2.00928 E+08	1.07909 E+08	1.40240 E+08	1.12127 E+05	2.05809 E+06
3	0.3	0	0	1.96578 E+08	1.10043 E+08	1.45903 E+08	1.12060 E+05	2.09856 E+06
4	0.4	0	0	1.93231 E+08	1.11469 E+08	1.49543 E+08	1.12025 E+05	2.08014 E+06
5	0.5	0	0	1.90546 E+08	1.12666 E+08	1.52501 E+08	1.12005 E+05	2.23557 E+06
6	1	0	0	1.85744 E+08	1.16574 E+08	1.58012 E+08	1.11954 E+05	1.99479 E+06
7	10	0	0	1.70252 E+08	1.45168 E+08	1.75271 E+08	1.11636 E+05	1.86244 E+06
8	100	0	0	1.47951 E+08	1.36904 E+08	2.08646 E+08	1.10268 E+05	2.31333 E+06
9	1000	0	0	9.51694 E+07	6.39179 E+07	2.88073 E+08	1.07290 E+05	3.73178 E+06

Acidity variation

Figure 16. Acidity of 1000 mD fault permeability model. This figure shows the distribution of pH in the CO_2 plume. The upper seal SSTN-1 showed a higher acidity and was similar to that observed at injection zone D-E. This is because a large permeability allows the CO_2 plume to move up due its specific gravity, particularly in the case of the 1000 mD permeability model.

basaltic rock released Fe^{+2}, Mg^{+2}, Ca^{+2} and Al^{+3} during the injection period and stopped afterwards due to the decrease in acidity. After the acidity decreased, the rate of CO_2 dissolution reached equilibrium with the deposition rate of solid phase CO_2 formed through Eqs. (1), (2), (3), (4), (5), and (6). The nature of the equilibrium varied depending on the location of CO_2 plume. In the case of the injection zone, the average time to arrive at the equilibrium point was 50 years from the starting point in 2016. This period was increased in models that had had high permeabilities (10, 100 and 1000 mD) because part of the CO_2 plume escaped from the injection zone to other zones through the fault. Consequently, the ability of the CO_2 plume to react with the basaltic rock was reduced. In the seal zones, a different equilibrium behavior was observed due to the downward migration of the CO_2 plume that corresponded with the

differences in specific gravity between the aqueous phase of CO_2 and the dissolved phase. Due to this, a small portion of the CO_2 plume in the dissolved phase moved up into upper seal SSTN-1 through the fault where the pH was still high. Subsequently, the equilibrium point occurred later in the upper seal than the lower seal SSTN-2 (Table 5). When the rate of CO_2 deposition exceeded the rate of dissolution, the third step in the kinetic reactions, mineralization, began to occur. Although CO_2 deposition began earlier, the mineralization rate was equal to the dissolution rate at the equilibrium point and then increased gradually to a maximum value at the end of the simulation period (Table 5).

In the injection zone, CO_2 precipitation increased in the presence of decreased permeability and forced the CO_2 plume to move horizontally within the zone towards areas with a higher porosity (average 14%) and

CO₂ Phase variation

CO2 Sequestration 1000 mD Permeability Model

CO2 Sequestration 0.1 m D Permeability Model

Figure 17. Distribution of the CO_2 phases over time for fault permeabilities values 0.1 mD and 1000 mD.For the fault permeability 0.1 mD, the seal effectively kept the supercritical CO_2 within the injection zone and its migration was horizontal. In this scenario, the dissolved CO_2 phase increased rapidly during the injection period and remained constant after injection through the end of simulation. For 1000 mD fault permeability, the seal allowed CO_2 to leak out of the injection zone. For this case, the maximum value of supercritical CO_2 was still low relative to that of the 0.1 mD case and double the amount of dissolved CO_2 for 0.1 mD case (2.97 EXP +09 mol vs. 1.55 EXP +09 mol). Mineral phase CO_2 in the case of 1000 mD was more than 0.1. However, most of the CO_2 in the mineral phase was observed outside of the injection and seal zones due to the low resistance of the seal zone.

permeability (1–200 mD). The activity in the seal zone was complementary to that in the injection zone. In the seal zone, the precipitation of calcite was proportional to fault permeability in both the upper and lower seal. However, the upper seal had lower values of precipitation than the lower seal due to differences in specific gravity of the aqueous phase, supercritical, and dissolved phase (Table 5). The important storage the faulted area especially in the onshore part of the basin could support small to intermediate projects around the CO_2 sources like a power stations and that support the feasibility and reduce storage costs.

8. Conclusions

Understanding the migration and chemical reactions associated with injected CO_2 was key to determining the effect of mineralization on leakage in the SGR basin. Variations in fault permeability greatly impacted the interaction of carbonic acid with the surrounding rock and

the resulting multi-phase CO_2 distribution in the formation. When considering the relatively small amount of 10 million m³/year CO_2 injected over the short period of 20 years, the critical range of fault permeability was effective for both reducing the vertical migration of the plume and maximizing the time for chemical reactions associated with mineralization. High fault permeability values supported the migration of CO_2 to the top of the model in a time period that was not long enough to allow for mineralization, especially at fault permeability values of 100 and 1000 mD. The low resistance of higher fault permeability values also allowed aqueous phase CO_2 to penetrate seal zones at the beginning of the simulation.

A permeability of 10 mD was the maximum value that would allow for a successful storage system. This is because in a scenario with a greater permeability, the migration of the CO_2 plume could penetrate the seal and some of the CO_2 plume would escape into the atmosphere. The critical values of fault permeability (0.1–1 mD) forced CO_2 in the aqueous

phase to remain within the reservoir zone (D-E) and allow ample time for the plume to form the carbonate minerals within the fault zone. Due to this, permeability values that fell within the critical range corresponded to effective mineralization occurring within the seal. CO_2 in the aqueous phase was located generally in the injection zone, while mineralization typically occurred in the seal zone. The resistance of the seal zones contained CO_2 as long as possible and enhanced the dissolution of aqueous CO_2.

Calcite dissolved at the beginning of the injection period then arrived at the equilibrium point where its dissolution rate was equal to the rate of deposition. Before equilibrium was reached, the plume migrated towards the seal, carrying calcite and kaolinite from the injection zone to the fault zone. During this process, kaolinite began to mineralize in the injection zone at the time of injection and continued to do so until the end of the simulation throughout all of the zones. The amount of kaolinite that mineralized during this process was dependent on fault permeability in the formation.

This study suggests that low fault permeabilities allowed for CO_2 migration in cases where no chemical reactions occurred, and that this migration could be contained by mineralization. This was evidenced by the observation that leakage associated with low fault permeability values decreased significantly when new minerals such as calcite and kaolinite were generated in the fault zone. Consequently, the opportunity for the CO_2 plume to migrate through the fault was reduced which provided an opportunity to sequester injected CO_2 in a reservoir with faults. Given that CO_2 mineralization is currently considered the safest way to store CO_2, this research provides more context for this safe storage mechanism within the reservoir but also suggests how to further stabilize storage through securing seal zones within a formation. The methods described in this study could be used for a variety of complex geological settings, particularly those impacted by tectonic activity, for which CO_2 storage is desired.

Declarations

Author contribution statement

Adil Alshammari: Conceived and designed the experiments; Performed the experiments; Analyzed and interpreted the data; Wrote the paper.

Venkat Lakshmi: Conceived and designed the experiments; Contributed reagents, materials, analysis tools or data.

Duke Brantley: Performed the experiments; Contributed reagents, materials, analysis tools or data.

Camelia C. Knapp: Analyzed and interpreted the data; Wrote the paper.

James H. Knapp: Contributed reagents, materials, analysis tools or data; Wrote the paper.

Funding statement

This work was supported by the U.S. Department of Energy, National Energy Technology Laboratory, and the University of South Carolina.

Data availability statement

The authors do not have permission to share data.

Declaration of interests statement

The authors declare no conflict of interest.

Additional information

No additional information is available for this paper.

References

Akintunde, O.M., et al., 2013. New constraints on buried Triassic basins and regional implications for subsurface CO2 storage from the SeisData6 seismic profile across the Southeast Georgia coastal plain. Environ. Geosci. 20 (1), 17–29.

Akintunde, O.M., Knapp, C., Knapp, J.H., 2017. Aki permeability prediction and distribution in the confined South Georgia rift red beds with implications for CO2 storage. In: AAPG 2017 Annual Convention and Exhibition. Houston.

Alfredsson, H.A., et al., 2008. CO2 sequestration in basaltic rock at the Hellisheidi site in SW Iceland: stratigraphy and chemical composition of the rocks at the injection site. Minerol. Magazin 72 (1), 1–5.

Aradóttir, E.S., et al., 2011. CarbFix: a CCS pilot project imitating and accelerating natural CO2 sequestration. Greenhouse Gases: Sci. Technol. 1 (2), 105–118.

Bachu, S., Adams, J.J., 2003. Bac Sequestration of CO2 in geological media in response to climate change: capacity of deep saline aquifers to sequester CO2 in solution. Energy Convers. Manag. 44 (20), 3151–3175.

Brantley, D.T., Shafer, J.M., Lakshmi, V., Waddell, M., 2015. The inclusion of faults in 3-D numerical simulation of carbon dioxide injection into the south Georgia rift basin, South Carolina. Int. J. Earth Sci. Geophys.

CMG, 2017. Advanced Compositional and Unconventional Reservoir Simulation. Users Guide. Retrieved from Computer modeling group Ltd, Calgary, Alberta. https://www.cmgl.ca/software.

Cumbest, R.J., 1998. Basement SurFace Faulting and Topography for Savannah River Site and Vicinity . Savannah River Site (US).No. WSRC-TR-98-00346.

Dabirian, R., et al., 2012. Mineral carbonation in peridotite rock for CO2 sequestration and a method of leakage reduction of CO2 in the rock. Nafta 63 (1-2), 44–48.

EA Al-Khdheeawi, S., et al., 2018. Impact of injected water salinity on CO2 storage efficiency in homogenous reservoirs. APPEA J. 58 (1), 44–50.

Frailey, S.M., Leetaru, H., 2009. Geological Factors Affecting CO2 Plume Distribution. Energy Procedia, pp. 3107–3112.

Gislason, S.R., 2010. Mineral sequestration of carbon dioxide in basalt: a pre-injection overview of the CarbFix project. Int. J. Greenh. Gas Control 4 (3), 537–545.

Gislason, S.R., et al., 2014. Rapid solubility and mineral storage of CO2 in basalt. Energy Proc. 63, 4561–4574.

Goldberg, D.S., et al., 2008. Carbon dioxide sequestration in deep-sea basalt. Proc. Natl. Acad. Sci. Unit. States Am. 105 (29), 9920–9925.

Goldberg, D.S., Kent, D.V., Olsen, P.E., 2010. Ervoirs for CO2 Sequestration in Central Atlantic Magmatic Province Basalts. National Academy of Sciences, pp. 1327–1332.

Goldberg, D., Slagle, A.L., 2009. A global assessment of deep-sea basalt sites for carbon sequestration. Energy Proc. 1 (1), 3675–3682.

Gutiérrez-Alonso, G., et al., 2008. Self-subduction of the Pangaean global plate. Nat. Geosci. 1 (8), 549–553.

Heffner, D.M., 2013. Tectonics of the South Georgia Rift. Retrieved from University of South Carolina, Columbia, SAC 29208. Doctoral Dissertation: http://scholarcommons.sc.edu/etd/1330.

Holloway, S., 2007. Carbon dioxide capture and geological storage. Philosophical Transactions of the Royal Society. Math. Phys. Eng. Sci. 1095–1107.

Khan, A.A., et al., 2015. Carbon dioxide capture characteristics from flue gas using aqueous 2-amino-2-methyl-1-propanol (AMP) and monoethanolamine (MEA) solutions in packed bed absorption and regeneration columns. Int. J. Greenh. Gas Control 32, 15–23.

Khatiwada, M., et al., 2012. A feasibility study of time-lapse seismic monitoring of CO2 sequestration in a layered basalt reservoir. J. Appl. Geophys. 82, 145–152.

King, P.B., 1971. Systematic pattern of Triassic dikes in the Appalachian region-second report. US Geol. Survey.

Klitgord, K.D., et al., 1988. A typical Atlantic-type or passive continental margin. In: Grow, J.A., Sheridan, R.E. (Eds.), U.S. Atlantic Continental Margin. The Geology of North America, pp. 2, 19-55.

Law, D.H.S., Bachu, S., 1996. Hydrogeological and numerical analysis of CO2 disposal in deep aquifers in the Alberta sedimentary basin. Energy Convers. Manag. 37 (6-8), 1167–1174.

Luo, S., et al., 2012. Effect of reactive surface area of minerals on mineralization trapping of CO2 2 in saline aquifers. Petrol. Sci. 9 (3), 400–407.

Marzoli, A., Renne, P.R., Piccirillo, E.M., Ernesto, M., Bellieni, G., De Min, A., 1999. Extensive 200-million-year-old continental flood basalts of the central atlantic magmatic province. Science 284 (5414), 616–618.

McBride, R.A., Moslow, T.F., 1991. Origin, evolution, and distribution of shoreface sand ridges, Atlantic inner shelf, USA. Mar. Geol. 97 (1-2), 57–85.

McGrail, B.P., et al., 2006. Potential for carbon dioxide sequestration in flood basalts. Journal of Geophysical Research. Solid Earth 111 (B12).

Melillo, J.M., 2014. Climate Change Impacts in the United States. Third National Climate Assessment, 52. Retrieved from globalchang.gov. https://www.globalchange.gov/sit

es/globalchange/files/Ch_0a_FrontMatter_ThirdNCA_GovtReviewDraft_Nov_22_2013_clean.pdf.

Nicol, A., Seebeck, H., Field, B., McNamara, D., Childs, C., Craig, J., Rolland, A., 2017. Fault Permeability and CO_2 Storage. Energy Procedia, pp. 3229–3236.

Oelkers, E.H., et al., 2008. Mineral carbonation of CO_2. Elements 4 (5), 333–337.

Pan, L., Oldenburg, C.M., Wu, Y.S., Pruess, K., 2009. Wellbore flow model for carbon dioxide and brine. Energy Proc. 71–78.

Rine, J.M., et al., 2014. Diagenetic and burial history of a portion of the late triassic South Georgia rift basin based on petrologic and isotopic (δ18O) analyses of sandstones from test borehole Rizer# 1, colleton county, SC. In: AAPG Annual Convention and Exhibition, 6. Houston, Texas, USA: April.

Rosa, D.R., Rosa, R.N., 2012. Heat as a by-product or sub-product of CO 2 storage in mafic and ultramafic rocks. Int. J. Glob. Warming 305–316.

Schaef, H.T., McGrail, B.P., 2009. Dissolution of Columbia River Basalt under mildly acidic conditions as a function of temperature: experimental results relevant to the geological sequestration of carbon dioxide. Appl. Geochem. 24 (5), 980–987.

Schlumberger, 2015. Petrel™ E&P Software. Retrieved *from Schlumberger:*. http://www.software.slb.com/products/platform/Pages/petrel.aspx.

Seifritz, W., 1990. CO 2 disposal by means of silicates. Nature 345 (6275), 486.

Snæbjörnsdóttir, S.Ó., Wiese, F., Fridriksson, T., Ármansson, H., Einarsson, G.M., Gislason, S.R., 2014. CO_2 storage potential of basaltic rocks in Iceland and the oceanic ridges. Energy Proc. 63, 4585–4600.

Stocker, T., 2014. Climate Change 2013: the Physical Science Basis. Cambridge University Press.

Xiong, W., Wells, R.K., Horner, J.A., Schaef, H.T., Skemer, P.A., Giammar, D.E., 2018. CO_2 mineral sequestration in naturally porous basalt. Environ. Sci. Technol. 142–147.

Yuan, Y., et al., 2022. Rapid mineralization of CO_2 with carbide slag in the constant-pressure and continuous-feed way and its reaction heat. Powder Technol. 398, 117148.

Ziegler, P.A., 2012. Evolution of Laurussia: a Study in Late Palaeozoic Plate Tectonics. Springer Science & Business Media.